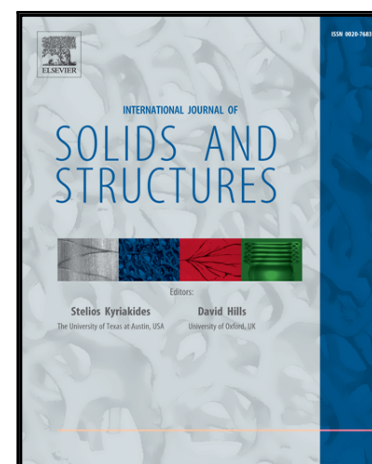


Accepted Manuscript

The incidence of slip system interactions on the deformation of FCC single crystals: system selection and segregation for local and non-local constitutive behavior

J.L. Dequiedt

PII: S0020-7683(18)30008-8
DOI: [10.1016/j.ijsolstr.2018.01.008](https://doi.org/10.1016/j.ijsolstr.2018.01.008)
Reference: SAS 9857



To appear in: *International Journal of Solids and Structures*

Received date: 27 September 2017
Revised date: 6 December 2017
Accepted date: 6 January 2018

Please cite this article as: J.L. Dequiedt, The incidence of slip system interactions on the deformation of FCC single crystals: system selection and segregation for local and non-local constitutive behavior, *International Journal of Solids and Structures* (2018), doi: [10.1016/j.ijsolstr.2018.01.008](https://doi.org/10.1016/j.ijsolstr.2018.01.008)

This is a PDF file of an unedited manuscript that has been accepted for publication. As a service to our customers we are providing this early version of the manuscript. The manuscript will undergo copyediting, typesetting, and review of the resulting proof before it is published in its final form. Please note that during the production process errors may be discovered which could affect the content, and all legal disclaimers that apply to the journal pertain.

Highlights

- System activation under prescribed deformation is influenced by their interactions
- Hierarchy of interactions drives system selection
- Segregation may take place in the form of band type patterns
- These phenomena are justified by linear stability analysis
- Gradient plasticity effects penalize some of the segregation modes

The incidence of slip system interactions on the deformation of FCC single crystals: system selection and segregation for local and non-local constitutive behavior.

J.L. Dequiedt¹.

CEA, DAM, DIF, F-91297 Arpaçon, France

Abstract:

In single-crystal plasticity, latent hardening between the different slip systems, coming from the interaction of dislocations, strongly influences the mechanical response under prescribed deformation. In this work, the selection of activated systems and their potential segregation in separated zones, taking place in a way which minimizes strain hardening due to system interactions, is investigated analytically for ductile FCC crystals. The crucial role of the respective intensity of the different interactions, estimated by dislocation dynamics simulations, is emphasized and, among them, the very strong collinear interaction between cross slip systems. The evolution of loading paths along lattice axes from symmetric to non-symmetric system activation, which reduces the number of systems, is triggered by uniform instability modes of the initial deformation framework. In the same trend, the segregation of systems in disconnected parts of the crystal, which tend to dissociate primarily strongly interacting pairs, is initiated by plane wave instability modes. Moreover, the introduction of gradient plasticity effects in the form of back stresses functions of the dislocation density tensor, not only introduces an internal length scale for the segregation process, but also brings a selection among the modes in a way which limits the induced incompatibility of the plastic strain field and, hence, the geometrically necessary dislocation (GND) density accumulation.

¹ Tel. : + 33 0 169264000

E-mail address : jean-lin.dequiedt@cea.fr

Keywords: Dislocation densities; Crystal plasticity; Strain gradient plasticity; Stability.

1. Introduction.

The role of slip system interactions on the deformation of single crystals under prescribed loading is well established. The interaction process between the dislocations acting on these different systems is at the origin of hardening and drives the stress-strain response of the material. The crystal having the propensity to accommodate the deformation by a mean that minimizes the stored energy, it will select and combine these systems in such a way as to reduce unfavorable interactions which have the highest hardening effect. The question has been addressed in Busso and Cailletaud (2005) for instance; they emphasized the crucial role of latent hardening moduli which measures the intensity of system interactions.

A first outcome is the selection of systems under prescribed deformation and, specifically, the evolution of symmetric orientations (i.e. loading along axes of symmetry of the crystal lattice), for which the equal activation of a high number of systems is expected. The number of systems being more than the one necessary to accommodate the deformation, the loading path deviates towards a non-symmetric deformation path in which some of the systems are progressively deactivated. This has been displayed, for instance, in Franciosi and Zaoui (1982) experiments on copper single crystals, in which only one part of favorably oriented systems is identified. A second consequence of system interactions is the development of non-homogeneous deformation patterns. When a single crystal is submitted to a prescribed deformation which necessarily combines several systems, these systems have the propensity to split into sub-groups activated in separated zones. This has been observed for various loading conditions: monotonous large deformations in the early works of Piercy et al. (1955) and Saimoto (1963) on brass and copper

respectively, cyclic loading by Jin and Winter (1984) but also for small amplitude deformations such as in Dmitrieva et al. (2009) who observed the formation of segregation bands in sheared copper. For large deformations (either monotonous or cyclic) the key role of dislocation substructures at microscopic scale (cell, walls,...) clearly appears from the observations. However, segregation observed in the early stages of deformation can be analyzed at the scale of continuum as has been done in a number of works: it was justified by energy considerations as a mean to minimize the plastic work expanded and as a consequence of latent hardening. The approach was developed by Ortiz and Repetto (1999) who postulated a sequential lamination process leading to zones of single slip and later by Petryk and Kurska (2013) who successfully predicted the band orientation in the experiments of Dmitrieva et al. (2009) on copper. In the same trend, Yalcinkaya et al. (2012) derived the hardening terms in the critical shear stresses from a non-convex free energy depending on slip on all systems; the potential energy thus reaches its minima on multiphase solutions which justifies segregation. All these works assumed a hardening matrix with higher coefficients for latent hardening than for self hardening, which penalizes multi-slip configurations.

However, both the slip system selection and the potential segregation process strongly depend on the hierarchy of latent hardening coefficients between all pairs of systems. Thus, a thorough investigation of this requires accurate data on their respective strengths. In this aim, dislocation dynamics (DD) simulations provide physical modeling of all kinds of interactions and lead to a precise estimation of the hardening coefficients.

In a previous study (Dequiedt et al., 2015), slip system segregation for copper FCC single crystals in biaxial stretching was analyzed in a continuum framework. However, one shortcoming

of approaches based on plastic work minimization is that they only hold when the incremental stress and strain are related through a symmetric tensor which is not systematically the case with physical interaction coefficients. For this reason, the onset of heterogeneous activation patterns was linked to critical eigenmodes of the homogeneous deformation of the crystal driven from a linear perturbation analysis. The interaction coefficients were taken from the work of Kubin et al. (2008). For a few crystal orientations, band type or more complex (spotty) segregation patterns were displayed by crystal plasticity simulations. Both numerical and analytical approaches showed that the partition process is driven by pairs of systems with the strongest interaction, namely pairs of cross slip systems when such pairs are activated.

The aim of the present work is to carry on further investigation on FCC single crystals under equibiaxial stretching. Various crystal orientations are investigated by tuning the normal to the stretching axes in the “standard triangle” of the crystal pole figure. Uniform deformation paths and the selection of slip systems are explored thanks to numerical simulation and their stability is investigated analytically. The switching from symmetric to non-symmetric system activation on the boundary of the standard triangle is justified by the existence of uniform instability modes of the initial symmetric solution.

Secondly, segregation is revisited for different orientations in the standard triangle (in the form of band type instability eigenmodes leading to lamellar substructures as has been done in Dequiedt et al., 2015) with evaluation of the incidence of non-local effects. Indeed, one shortcoming of the local continuum approach developed in Dequiedt et al. (2015) is the lack of an internal length scale for the segregation process, which is clearly not physical. In crystal plasticity, non-local effects stem from the incompatibility of plastic deformation fields leading to the storage of polar

dislocation densities. The local arrangements of these dislocations generate stresses which affect plastic slip. In the aim of evaluating size effects in the segregation process, the former stability analysis is extended by adding gradient terms to the constitutive model as functions of a dislocation density tensor in the framework developed by Gurtin (2002) and coworkers. It then yields wavelength dependent growth rates for the instability modes each time the partition of systems is accompanied by plastic strain field incompatibility.

The constitutive model and the related instability analysis, including gradient effects, are presented in Section 2. Section 3 is devoted to homogeneous deformation paths; the set of slip systems activated in different points of the standard triangle is identified and the number of cross slip pairs is emphasized. Specifically, the case of symmetric configurations is detailed and the instability of symmetric system activation paths is established. Section 4 investigates the onset of segregation from stable homogeneous deformation paths and analyzes the incidence of gradient effects on segregation modes.

2. Framework.

The single crystal constitutive model in its local form, which is detailed in Dequiedt et al. (2015), is recalled in Section 2.1. Small deformation formalism is retained. Indeed, the former study showed that geometric effects, i.e. the rotation of slip systems to favorable orientations that lowers slip resistance (as emphasized in Asaro, 1979 for instance), did not drive segregation in the early stages of loading and therefore, finite deformation terms were of minor influence. As in Dequiedt et al. (2015), a viscoplastic formulation is adopted which regularizes the constitutive behavior in the vicinity of yield stresses (critical shear stresses in crystal plasticity) and allows for

a linear perturbation analysis under conditions which will be detailed. The main features of the linear stability analysis (LSA), considering either uniform or band type (i.e. plane wave) eigenmodes, are presented in Section 2.2. Gradient effects are next introduced in Section 2.3.

2.1. Local constitutive model.

The small deformation elasto-plastic formalism is based on the additive decomposition of the displacement gradient into an elastic and a plastic part:

$$\mathbf{U} = \mathbf{grad}(\mathbf{u}) = \mathbf{U}^e + \mathbf{U}^p. \quad (1)$$

The elastic transformation can be split into its symmetric (deformation) and skew-symmetric (rotation) parts and the elastic-plastic decomposition (1) is such that the elastic rotation $\boldsymbol{\omega}^e$ is the rotation of the crystal lattice:

$$\mathbf{U}^e = \boldsymbol{\varepsilon}^e + \boldsymbol{\omega}^e \quad (2)$$

The elastic behavior is given by a linear relation between the Cauchy stress and the elastic strain:

$$\boldsymbol{\sigma} = \mathbf{C} : \boldsymbol{\varepsilon}^e. \quad (3)$$

For cubic single crystals, the elastic stiffness tensor \mathbf{C} has a cubic symmetry and is defined by the three parameters C_{11} , C_{12} , C_{44} (using Voigt indices). For FCC copper, they are taken from Simmons and Wang (1971) (Table 1).

Table 1
Elastic moduli for copper.

C_{11}	C_{12}	C_{44}
168.4 GPa	121.4 GPa	75.4 GPa

The plastic transformation rate is given by summing the plastic shearing rates over all slip systems (superimposed dot is used for time derivatives):

$$\dot{\mathbf{U}}^p = \sum_{\alpha} \dot{\gamma}^{\alpha} \mathbf{S}^{\alpha} \quad \text{with} \quad \mathbf{S}^{\alpha} = \mathbf{m}^{\alpha} \otimes \mathbf{n}^{\alpha}. \quad (4)$$

\mathbf{m}^{α} and \mathbf{n}^{α} are orthonormal unit vectors that define, respectively, the slip direction and slip plane normal.

The plastic shearing on slip system (α) is governed by the resolved shear stress:

$$\tau^{\alpha} = \boldsymbol{\sigma} : \mathbf{S}^{\alpha}, \quad (5)$$

and the shearing rate $\dot{\gamma}^{\alpha}$ is ruled by a viscoplastic power law formulation; it is positive or negative depending on the sign of the resolved shear stress:

$$\dot{\gamma}^{\alpha} = \dot{\gamma}_0 \operatorname{sgn}(\tau^{\alpha}) \left(\frac{|\tau^{\alpha}|}{\tau_c^{\alpha}} \right)^{1/m}, \quad (6)$$

with $\dot{\gamma}_0$ and m two material parameters.

The plastic flow can be re-formulated considering oriented slip systems, the oriented slip direction $\hat{\mathbf{m}}^{\alpha}$ being \mathbf{m}^{α} or $-\mathbf{m}^{\alpha}$ depending on whether the resolved shear stress τ^{α} is positive or negative respectively:

$$\begin{aligned} \dot{\mathbf{U}}^p &= \sum_{\alpha} \hat{\gamma}^{\alpha} \hat{\mathbf{S}}^{\alpha} \quad \text{with} \quad \hat{\mathbf{S}}^{\alpha} = \hat{\mathbf{m}}^{\alpha} \otimes \mathbf{n}^{\alpha}. \\ \hat{\gamma}^{\alpha} &= \dot{\gamma}_0 \left(\frac{\hat{\tau}^{\alpha}}{\tau_c^{\alpha}} \right)^{1/m} \quad \text{with} \quad \hat{\tau}^{\alpha} = |\tau^{\alpha}| = \boldsymbol{\sigma} : \hat{\mathbf{S}}^{\alpha}. \end{aligned} \quad (7)$$

The critical shear stresses τ_c^{α} , evolving with strain hardening as a consequence of dislocation interactions and storage, are given by a generalized storage-recovery model (Teodosiu et al. (1991)). They are related to the stored dislocation densities of all slip systems (β) using an extended forest type formulation proposed by Franciosi et al. (1980) and an interaction matrix

$a^{\alpha\beta}$. A constant stress τ_0 is also added in order to integrate glide resistance in the absence of stored dislocations (due to point defects, for instance):

$$\tau_c^\alpha = \tau_0 + \mu b \sqrt{\sum_\beta a^{\alpha\beta} \rho^\beta}, \quad (8)$$

where b is the Burgers vector and μ a shear modulus taken as the energy coefficient for screw dislocations in cubic crystals (Kubin, 2013, p. 240):

$$\mu = \sqrt{C_{44} \left(\frac{C_{11} - C_{12}}{2} \right)}. \quad (9)$$

Then, the evolution of the dislocation density $\dot{\rho}^\alpha$ is proportional to the amplitude of the plastic shearing rate $\hat{\gamma}^\alpha$:

$$\dot{\rho}^\alpha = \frac{1}{b} \left(\sqrt{\sum_\beta d^{\alpha\beta} \rho^\beta} - 2y_c \rho^\alpha \right) \hat{\gamma}^\alpha. \quad (10)$$

The first term expresses the dislocation storage arising from the pinning of mobile dislocations by the dislocation forest. The mean free path coefficients $d^{\alpha\beta}$ depend on the interaction coefficients $a^{\alpha\beta}$. For intersecting and coplanar slip systems, one has respectively:

$$d^{\alpha\beta} = \frac{a^{\alpha\beta}}{k_c^2} \quad \text{and} \quad d^{\alpha\beta} = \frac{a^{\alpha\beta}}{k_{nc}^2}. \quad (11)$$

The second term in Eq. (10) describes screw dislocation annihilations during dynamic recovery.

In FCC metals, there are twelve slip systems and four slip planes. The interaction matrix, which is explicited in Dequiedt et al. (2015), contains six different coefficients related to the six types of interactions between dislocations:

- $a^{\alpha\alpha} = a_0'$ (self interaction),
- $a^{\alpha\beta} = a_1^{copla}$ if $\mathbf{n}^\alpha = \mathbf{n}^\beta$ and $\mathbf{m}^\alpha \neq \mathbf{m}^\beta$ (dipolar interaction),
- $a^{\alpha\beta} = a_1^{ortho}$ if $\mathbf{n}^\alpha \neq \mathbf{n}^\beta$ and $\mathbf{m}^\alpha \perp \mathbf{m}^\beta$ (Hirth lock),
- $a^{\alpha\beta} = a_1^{coli}$ if $\mathbf{n}^\alpha \neq \mathbf{n}^\beta$ and $\mathbf{m}^\alpha = \mathbf{m}^\beta$ (collinear interaction),
- $a^{\alpha\beta} = a_2$ if $\mathbf{n}^\alpha \neq \mathbf{n}^\beta$, $\mathbf{m}^\alpha \neq \mathbf{m}^\beta$ and the two slip planes have one of the two slip directions in common (glissile junction),
- $a^{\alpha\beta} = a_3$ for $\mathbf{n}^\alpha \neq \mathbf{n}^\beta$ and $\mathbf{m}^\alpha \neq \mathbf{m}^\beta$ in other cases (Lomer lock).

These coefficients were evaluated by dislocation dynamics simulations (Devincre et al. (2006); and Kubin et al. (2008)). The values of the coefficients adopted in this study are given in Kubin et al. (2008) (cf. Table 2) for all FCC crystals². The collinear interaction is by far the strongest: as was noticed in a previous work (Madec et al. (2003)), it induces a very strong latent hardening between cross slip systems.

² Recent DD simulations by Madec and Kubin (2017) showed that the interaction coefficients depend in fact on the material essentially through its “effective” Poisson ratio (derived from the ratio between screw and edge dislocation line energies). For some materials, the discrepancy between the different coefficients could be higher than predicted in Kubin et al. (2008). Moreover, they displayed the non-symmetry of the interaction matrix due to the non-symmetric role of the two systems forming a glissile junction. However, the order of coefficients is not modified significantly and the set given in Table 2 is kept for this work.

Table 2

Interaction coefficients (Kubin et al. (2008)).

a_0'	a_1^{copla}	a_1^{ortho}	a_1^{coli}	a_2	a_3
0.122	0.122	0.07	0.625	0.137	0.122

The initial dislocation density for all systems is taken as $\rho_0 = 10^8 \text{ m}^{-2}$. Other parameters of the storage-recovery model are taken from Kubin et al. (2008) and the parameters for the viscoplastic law are taken from Kalidindi and Anand (1992) (cf. Table 3).³

Table 3

Parameters of the generalized storage-recovery model for copper.

y_c	τ_0	$\dot{\gamma}_0$	m	b	k_c	k_{nc}
$10^* b$	1 MPa	10^{-3} s^{-1}	0.012	$2.56 \cdot 10^{-10} \text{ m}$	12	180

2.2. Instability analysis.

The departure from symmetric system activation and the onset of segregation for the single crystal in biaxial stretching is assumed to be ruled by the instability of reference deformation paths and triggered by some perturbation introduced at a given time t_0 of loading. The existence of perturbations growing with time is searched by a linear stability analysis (LSA) which has still been applied to single crystal plasticity by Molinari (1988). The basic (uniform) and disturbed (uniform or non-uniform) solution are defined by their material velocity fields $\mathbf{v}_0(\mathbf{x}, t)$ and

³ The dynamic recovery length y_c is of little influence in this study concerned with small deformation loadings; an average value of $y_c/b = 10$ was retained. A more precise evaluation of this parameter is provided in Kubin et al. (2009).

$\mathbf{v}_*(\mathbf{x}, t) = \mathbf{v}_0(\mathbf{x}, t) + \delta\mathbf{v}(\mathbf{x}, t)$; for these two solutions, all mechanical variables are supposed to satisfy periodic boundary conditions on a single crystal volume Ω consistent with a prescribed average displacement gradient $\mathbf{U}_0(t)$; . The constitutive equations are written for \mathbf{v}_0 and \mathbf{v}_* leading to evolution equations for the perturbation $\delta\mathbf{v}$.

Inertia is neglected and a time scale separation condition is assumed (implicit in many linear stability analyses), namely that the perturbation grows with a time scale an order of magnitude shorter than the characteristic time of the basic solution. In these conditions, it satisfies time differential equations with “frozen” (time independent) coefficients and can be searched in the form of eigenmodes growing exponentially (the growth rate η being either real or complex). For any scalar or tensorial state variable related with the perturbation:

$$\delta A(\mathbf{x}, t) = \tilde{\delta A}(\mathbf{x}) \exp(\eta t). \quad (12)$$

Instability modes are such that $\text{Re}(\eta) > 0$.

Moreover, time scale separation condition implies that the relative evolution of critical shear stresses, dislocation densities and shearing rates for the basic solution satisfy (subscript 0 is omitted here and henceforth for the basic solution):

$$\frac{\dot{\tau}_c^\alpha}{\tau_c^\alpha} \ll \eta \quad \frac{\dot{\rho}^\alpha}{\rho^\alpha} \ll \eta \quad \frac{\dot{\dot{\gamma}}^\alpha}{\dot{\gamma}^\alpha} \ll \eta \quad (13)$$

Although preserving the viscoplastic character of the constitutive behaviour for both the basic solution and perturbation, this involves some simplifications in the relations between the perturbations on the former quantities as we shall see in the following.

The elastic behavior yields (owing the minor symmetry of tensor \mathbf{C}):

$$\delta\boldsymbol{\sigma} = \mathbf{C} : (\delta\boldsymbol{\varepsilon} - \delta\boldsymbol{\varepsilon}^p) = \mathbf{C} : (\delta\dot{\mathbf{U}} - \delta\dot{\mathbf{U}}^p). \quad (14)$$

We assume that, for each slip system, shearing takes place in the same sense for both the basic and disturbed solution, which is a condition for differentiability of the constitutive equations and validity of the linear perturbation analysis. Substantially, for given initial amplitudes of the shearing rate perturbations $\delta\hat{\dot{\gamma}}^\alpha(\mathbf{x}, t_0)$, the time interval Δt of validity of the LSA is such that these perturbations remain lower than the basic shearing rates⁴:

$$\max_{\mathbf{x} \in \Omega} \left(\left| \delta\hat{\dot{\gamma}}^\alpha(\mathbf{x}, t_0) \right| \right) \exp(\eta \Delta t) < \hat{\dot{\gamma}}^\alpha(t_0) \quad \text{for all slip systems } (\alpha). \quad (15)$$

Then the perturbations on plastic transformation and resolved shear stresses satisfy:

$$\delta\dot{\mathbf{U}}^p = \sum_{\alpha} \delta\hat{\dot{\gamma}}^\alpha \hat{\mathbf{S}}^\alpha \quad \text{and} \quad \delta\hat{\tau}^\alpha = \delta\boldsymbol{\sigma} : \hat{\mathbf{S}}^\alpha \quad \text{with} \quad \hat{\mathbf{S}}^\alpha = \frac{\dot{\gamma}^\alpha}{|\dot{\gamma}^\alpha|} \mathbf{S}^\alpha = \frac{\dot{\gamma}_*^\alpha}{|\dot{\gamma}_*^\alpha|} \mathbf{S}^\alpha. \quad (16)$$

The viscoplastic flow rule (7) gives for the perturbation:

$$\delta\hat{\tau}^\alpha = \delta\tau_c^\alpha \left(\frac{\hat{\dot{\gamma}}^\alpha}{\dot{\gamma}_0} \right)^m + m\tau_c^\alpha \frac{\delta\hat{\dot{\gamma}}^\alpha}{\dot{\gamma}_0} \left(\frac{\hat{\dot{\gamma}}^\alpha}{\dot{\gamma}_0} \right)^{m-1}. \quad (17)$$

⁴ For rate-independent plasticity, conditions of the same kind ensure that bifurcations remain in the plastic domain; a general discussion can be found in Bigoni and Petryk (2002).

Owing relations (13), time derivation of Eq. (17) gives:

$$\delta \dot{\tau}_c^\alpha = \delta \dot{\tau}_c^\alpha \left(\frac{\hat{\gamma}^\alpha}{\dot{\gamma}_0} \right)^m + \delta \hat{\gamma}^\alpha \frac{m \tau_c^\alpha \eta}{\dot{\gamma}_0} \left(\frac{\hat{\gamma}^\alpha}{\dot{\gamma}_0} \right)^{m-1}. \quad (18)$$

The expression of critical shear stresses (8) gives for the perturbation:

$$\delta \tau_c^\alpha = \sum_\beta \frac{\mu b a^{\alpha\beta}}{2 \sqrt{\sum_\gamma a^{\alpha\gamma} \rho^\gamma}} \delta \rho^\beta \quad (19)$$

Assuming that relation (13) holds for any function $g(\rho^\alpha)$ of dislocation densities linked with the basic solution, namely that:

$$\frac{1}{g(\rho^\alpha)} \left(\frac{d}{dt} (g(\rho^\alpha)) \right) \ll \eta, \quad (20)$$

time derivation of (19) yields:

$$\delta \dot{\tau}_c^\alpha = \sum_\beta \frac{\mu b a^{\alpha\beta}}{2 \sqrt{\sum_\gamma a^{\alpha\gamma} \rho^\gamma}} \delta \dot{\rho}^\beta \quad (21)$$

Eq. (10) between slip rates and dislocation densities can be inverted to:

$$\hat{\gamma}^\alpha = g^\alpha(\rho^\beta) \dot{\rho}^\alpha \quad \text{with:} \quad g^\alpha(\rho^\beta) = b \left(\sqrt{\sum_\beta d^{\alpha\beta} \rho^\beta} - 2 y_c \rho^\alpha \right)^{-1} \quad (22)$$

For the perturbation:

$$\delta \hat{\gamma}^\alpha = g^\alpha(\rho^\beta) \delta \dot{\rho}^\alpha + \left(\sum_\beta \frac{\partial g^\alpha}{\partial \rho^\beta} \delta \rho^\beta \right) \dot{\rho}^\alpha \quad (23)$$

All partial derivatives $\partial g^\alpha / \partial \rho^\beta$ being of the same order, the second term in (23) is of the same order as:

$$\left(\sum_{\beta} \delta \rho^\beta \right) \frac{\partial g^\alpha}{\partial \rho^\alpha} \dot{\rho}^\alpha < \left(\sum_{\beta} \delta \rho^\beta \right) \left(\frac{dg^\alpha}{dt} \right), \quad (24)$$

and, by virtue of (20), can be neglected.

Eqs. (21) and (23) yield a relation between the perturbations on the critical shear stresses and slip rates involving a tangent hardening matrix $H_{\alpha\beta}$:

$$\delta \dot{\tau}_c^\alpha = \sum_{\beta} H_{\alpha\beta} \delta \dot{\gamma}^\beta \quad \text{with} \quad H_{\alpha\beta} = \mu \left(\frac{\sqrt{\sum_{\gamma} d^{\beta\gamma} \rho^\gamma} - 2 y_c \rho^\beta}{2 \sqrt{\sum_{\gamma} a^{\alpha\gamma} \rho^\gamma}} \right) a^{\alpha\beta}. \quad (25)$$

Combination of Eqs. (14)-(25) gives the following system relating slip rates and velocity gradient for the perturbation:

$$\sum_{\beta} \mathbb{N}_{\alpha\beta}(\eta) \delta \dot{\gamma}^\beta = (\mathbf{C} : \hat{\mathbf{S}}^\alpha) : \delta \dot{\mathbf{U}}. \quad (26)$$

The components of matrix $\mathbb{N}(\eta)$ (introduced by Pierce et al. (1982) in the rate-independent case) are (with $\delta_{\alpha\beta}$ for Kronecker delta symbol):

$$\mathbb{N}_{\alpha\beta}(\eta) = \left(\frac{\dot{\gamma}^\alpha}{\dot{\gamma}_0} \right)^m \left(H_{\alpha\beta} + \frac{m \tau_c^\alpha}{\dot{\gamma}^\alpha} \eta \delta_{\alpha\beta} \right) - (\mathbf{C} : \hat{\mathbf{S}}^\alpha) : \hat{\mathbf{S}}^\beta. \quad (27)$$

For all values of the growth rate for which matrix $\mathbb{N}(\eta)$ is invertible, the incremental relation between the perturbation in stress and in displacement gradient is written in the form:

$$\delta \boldsymbol{\sigma} = \mathbf{L}(\eta) : \delta \dot{\mathbf{U}} \quad \text{with} \quad \mathbf{L}(\eta) = \mathbf{C} - \sum_{\alpha,\beta} \mathbb{N}_{\alpha\beta}^{-1}(\eta) (\mathbf{C} : \hat{\mathbf{S}}^\alpha) \otimes (\mathbf{C} : \hat{\mathbf{S}}^\beta). \quad (28)$$

Equilibrium yields:

$$\operatorname{div}(\delta \tilde{\sigma}) = 0. \quad (29)$$

Let us mention that (29) implies:

$$\frac{1}{2} \int_{\Omega} \delta \tilde{\sigma} : \delta \dot{\mathbf{U}} \, d\Omega = \frac{1}{2} \int_{\Omega} (\delta \dot{\mathbf{U}} : \mathbf{L}(\eta) : \delta \dot{\mathbf{U}}) \, d\Omega = 0 \quad (30)$$

Eq. (30) links the existence of the perturbed solution to the loss of convexity of a bilinear potential function defined on Ω as has been done for bifurcation problems in the rate-independent case by Petryk and Kurska (2013) or Kratochvil and Kruzik (2015) for instance.

However equivalence of (29) and (30) only holds when the tangent modulus $\mathbf{L}(\eta)$ is symmetric (as was noticed in various studies such as Bigoni and Hueckel (1991) or Neilsen and Schreyer (1993)) which is not the case here. Contrary to what has been displayed in previous works (Havner and Shalaby (1977), Pierce et al. (1982), Petryk and Kurska (2011) among others), the lack of symmetry of $\mathbf{L}(\eta)$ is not linked to geometric effects (emerging in a finite deformation framework) but to the lack of symmetry of the hardening matrix itself. Although the interaction matrix $a^{\alpha\beta}$ has been assumed symmetric (cf. Section 2.1)⁵, $H_{\alpha\beta}$ is not, due to its dependence on dislocation densities. Since this work focuses on the incidence of dislocation interactions, forced symmetrization has not been achieved.

Departure from symmetric loading paths is ruled by uniform perturbations on the set of slip rates consistent with the imposed displacement gradient: $\delta \mathbf{U}(t) \equiv 0$.

⁵ The influence of the non-symmetry of $a^{\alpha\beta}$ on instability (Madec and Kubin, 2017) is left for future work.

By virtue of Eq. (26), such eigenmodes satisfy:

$$\sum_{\beta} \mathbb{S}_{\alpha\beta}(\eta) \delta \hat{\gamma}^{\beta} = 0. \quad (31)$$

One or several mode exists with growth rate η such that:

$$\det(\mathbb{S}(\eta)) = 0. \quad (32)$$

The mode is defined by the set of slip rates which is the eigenvector of matrix $\mathbb{S}(\eta)$ associated with the null eigenvalue.

By another way, band type segregation is ruled by plane wave perturbations, periodic in direction \mathbf{N} (which is the normal to the bands) with wave number k (see Molinari, 1988 for instance). The perturbation expresses for the material velocity and velocity gradient (i is the unit imaginary number such that $i^2 = -1$ and \mathbf{M} is the displacement direction):

$$\begin{aligned} \delta \mathbf{v} &= \delta \tilde{v} \exp(ik(\mathbf{x} \cdot \mathbf{N})) \exp(\eta t) \mathbf{M}, \\ \delta \dot{\mathbf{U}} &= \mathbf{grad}(\delta \mathbf{v}) = ik \delta \tilde{v} \exp(ik(\mathbf{x} \cdot \mathbf{N})) \exp(\eta t) (\mathbf{M} \otimes \mathbf{N}). \end{aligned} \quad (33)$$

Shearing rate perturbations are searched in the same form:

$$\delta \hat{\gamma}^{\alpha} = ik \delta \tilde{\gamma}^{\alpha} \exp(ik(\mathbf{x} \cdot \mathbf{N})) \exp(\eta t) \quad (34)$$

Eq. (29) gives for the stress perturbation (Rice, 1976):

$$\mathbf{N} \cdot \delta \tilde{\boldsymbol{\sigma}} = 0. \quad (35)$$

By Eq. (28), a band type eigenmode with growth rate η does exist if:

$$(\mathbf{N} \cdot \mathbf{L}(\eta) \cdot \mathbf{N}) \cdot \mathbf{M} = 0. \quad (36)$$

For each orientation \mathbf{N} , one or several mode exists with growth rate η such that:

$$\det(\mathbf{N} \cdot \mathbf{L}(\eta) \cdot \mathbf{N}) = 0. \quad (37)$$

The mode is defined by the displacement direction \mathbf{M} which is the eigenvector of the so-called “acoustic tensor” $(\mathbf{N} \cdot \mathbf{L}(\eta) \cdot \mathbf{N})$ associated with the null eigenvalue.

Both the deviation from the symmetric deformation paths and the onset of segregation are governed by the eigenmodes with the highest growth rates η .

2.3. *Non-local effects.*

In crystal plasticity, non-local (gradient) effects can be explained by the fact that the gradients of plastic slip induce incompatibility of the plastic deformation field which has to be accommodated by polar dislocation densities (usually called “geometrically necessary dislocation” (GND) densities). An additional stored energy and, subsequently, microforces are associated with these densities. They are drawn from the statistical theory of dislocations and linked to spatial correlations functions (see for instance Groma et al., 2003). At the scale of continuum, they are introduced in the form of a free energy function of GND densities (Gurtin, 2002) or directly in the form of back stress terms in the flow rules (Evers et al., 2004, or Kuroda and Tvergaard, 2008, among others). In the following, the framework proposed by Gurtin and co-workers is retained; details are given in the different papers of the authors.

A measure of GND densities is given by a dislocation density tensor (Nye, 1953) which quantifies the non-closure of Burgers circuits induced by plastic deformation (see Cermelli and Gurtin, 2001, for instance) and is defined by:

$$\mathbf{G} = \mathbf{curl}(\mathbf{U}^p) = -\mathbf{curl}(\mathbf{U}^e). \quad (38)$$

It also reads as a function of slip gradients (using Eq. (4)):

$$\mathbf{G} = \sum_{\alpha} \mathbf{m}^{\alpha} \otimes (\mathbf{grad}(\gamma^{\alpha}) \times \mathbf{n}^{\alpha}). \quad (39)$$

The non-local constitutive model is derived following Gurtin and Needleman (2005). Plastic flow on each slip system is governed by conditions of equilibrium for gliding dislocations between external stresses (which equal resolved shear stresses once projected on the slip system) and microforces governing slip resistance. The latter consist in scalar forces π^{α} (due to forest dislocations, obstacles,...) expanding power the shearing rates and vector stresses ξ^{α} expanding power on the shearing rate gradients.

Both macroforce balance and plastic flow conditions are written in the form of an extended principle of virtual power in which virtual material velocity $\hat{\mathbf{v}}$ and virtual shearing rate $\hat{\gamma}^{\alpha}$ fields satisfy periodic boundary conditions on Ω and are specified independently. The virtual power of internal forces is the sum of a power expanded by elastic deformation and a power expanded by slip and writes (Gurtin and Needleman, 2005):

$$P_{\text{int}}(\hat{\mathbf{v}}, \hat{\gamma}^{\alpha}) = - \int_{\Omega} \boldsymbol{\sigma} : (\hat{\mathbf{U}} - \hat{\mathbf{U}}^p) d\Omega - \sum_{\alpha} \int_{\Omega} (\pi^{\alpha} \hat{\gamma}^{\alpha} + \xi^{\alpha} \cdot \mathbf{grad}(\hat{\gamma}^{\alpha})) d\Omega, \quad (40)$$

in which a velocity gradient and a plastic transformation rate are defined for the virtual fields by:

$$\hat{\mathbf{U}} = \mathbf{grad}(\hat{\mathbf{v}}) \quad \text{and} \quad \hat{\mathbf{U}}^p = \sum_{\alpha} \hat{\gamma}^{\alpha} \mathbf{S}^{\alpha}. \quad (41)$$

The principle of virtual power leads after integration by parts, for each slip system, to the balance of forces governing slip (boundary terms lead to periodicity conditions on vector stresses ξ^{α}):

$$\tau^{\alpha} - \pi^{\alpha} + \text{div}(\xi^{\alpha}) = 0. \quad (42)$$

π^α is the slip resistance in the absence of gradient effects and let us assume that it is related to the shearing rate $\dot{\gamma}^\alpha$ by Eq. (6):

$$\dot{\gamma}^\alpha = \dot{\gamma}_0 \operatorname{sgn}(\pi^\alpha) \left(\frac{|\pi^\alpha|}{\tau_c^\alpha} \right)^{1/m}. \quad (43)$$

Gurtin and co-workers (Gurtin and Needleman, 2005) derive the vector stresses ξ^α from a free energy function of \mathbf{G} ; this energy expresses in its simplest form (in which L is the length scale parameter of the non-local model):

$$\Psi(\mathbf{G}) = \frac{1}{2} S_0 L^2 \|\mathbf{G}\|^2 \quad \text{with} \quad \|\mathbf{G}\|^2 = \mathbf{G} : \mathbf{G}. \quad (44)$$

S_0 has dimension of stress and can be set equal to the shear modulus ($S_0 = \mu$) without loss of generality, the intensity of the free energy being captured by L . The positivity of plastic dissipation linked with gradient effects yields:

$$\sum_\alpha \xi^\alpha \cdot \operatorname{grad}(\dot{\gamma}^\alpha) - \frac{\partial \Psi}{\partial \mathbf{G}} : \dot{\mathbf{G}} \geq 0. \quad (45)$$

Following Gurtin and Needleman (2005), we state that vector stresses are non-dissipative; subsequently:

$$\xi^\alpha = \mathbf{n}^\alpha \times (\mathbf{T}^T \cdot \mathbf{m}^\alpha), \quad (46)$$

with \mathbf{T}^T the transpose of tensor \mathbf{T} defined by $\mathbf{T} = \partial \Psi / \partial \mathbf{G} = \mu L^2 \mathbf{G}$.

Combining Eq. (42), (43) and (46), it comes that vector stresses introduce a backstress term τ_b^α in the flow rule; this stress is a linear function of the second order space derivatives of the slips γ^α :

$$\dot{\gamma}^\alpha = \dot{\gamma}_0 \operatorname{sgn}(\tau^\alpha - \tau_b^\alpha) \left(\frac{|\tau^\alpha - \tau_b^\alpha|}{\tau_c^\alpha} \right)^{1/m}, \quad (47)$$

with:

$$\tau_b^\alpha = -\operatorname{div}(\xi^\alpha) = -\mu L^2 \operatorname{div}(\mathbf{n}^\alpha \times (\mathbf{G}^T \cdot \mathbf{m}^\alpha)). \quad (48)$$

Assuming that each slip system is activated in the same sense everywhere in Ω in the cases considered here, the non-local model is re-written considering oriented slip systems:

$$\hat{\gamma}^\alpha = \dot{\gamma}_0 \left(\frac{\hat{\tau}^\alpha - \hat{\tau}_b^\alpha}{\tau_c^\alpha} \right)^{1/m},$$

with:

$$\hat{\tau}_b^\alpha = -\mu L^2 \operatorname{div}(\mathbf{n}^\alpha \times (\mathbf{G}^T \cdot \hat{\mathbf{m}}^\alpha)) \quad \text{and} \quad \mathbf{G} = \sum_{\beta} \hat{\mathbf{m}}^\beta \otimes (\operatorname{grad}(\hat{\gamma}^\beta) \times \mathbf{n}^\beta). \quad (49)$$

In the linear perturbation analysis, time derivation of the viscoplastic flow rule now yields:

$$\delta \dot{\tau}^\alpha = \delta \dot{\tau}_c^\alpha \left(\frac{\hat{\gamma}^\alpha}{\dot{\gamma}_0} \right)^m + \delta \hat{\gamma}^\alpha \frac{m \tau_c^\alpha \eta}{\dot{\gamma}_0} \left(\frac{\hat{\gamma}^\alpha}{\dot{\gamma}_0} \right)^{m-1} + \delta \dot{\tau}_b^\alpha. \quad (50)$$

The dislocation density tensor and thus the backstress term for the plane wave perturbation are functions of the wavenumber k and direction \mathbf{N} :

$$\begin{aligned} \delta \dot{\mathbf{G}} &= ik \sum_{\beta} \delta \hat{\gamma}^\beta (\hat{\mathbf{m}}^\beta \otimes (\mathbf{N} \times \mathbf{n}^\beta)), \\ \delta \dot{\tau}_b^\alpha &= \mu k^2 L^2 \sum_{\beta} \delta \hat{\gamma}^\beta (\hat{\mathbf{m}}^\beta \cdot \hat{\mathbf{m}}^\alpha) [(\mathbf{N} \times \mathbf{n}^\beta) \cdot (\mathbf{N} \times \mathbf{n}^\alpha)], \end{aligned} \quad (51)$$

Combining Eqs. (14)-(16), (25) and (50)-(51) gives the following system relating slip rates and velocity gradient for the plane wave perturbation:

$$\sum_{\beta} \mathbb{S}_{\alpha\beta}(\eta, \bar{k}, \mathbf{N}) \delta \dot{\gamma}^{\beta} = (\mathbf{C} : \hat{\mathbf{S}}^{\alpha}) : \delta \dot{\mathbf{U}}. \quad (52)$$

Matrix \mathbb{S} now depends on the growth rate η , non-dimensional wave number $\bar{k} = kL$ and direction \mathbf{N} :

$$\mathbb{S}_{\alpha\beta}(\eta, \bar{k}, \mathbf{N}) = \left(\frac{\dot{\gamma}^{\alpha}}{\dot{\gamma}_0} \right)^m \left(H_{\alpha\beta} + \frac{m \tau_c^{\alpha}}{\dot{\gamma}^{\alpha}} \eta \delta_{\alpha\beta} \right) - (\mathbf{C} : \hat{\mathbf{S}}^{\alpha}) : \hat{\mathbf{S}}^{\beta} + \mu \bar{k}^2 (\hat{\mathbf{m}}^{\beta} \cdot \hat{\mathbf{m}}^{\alpha}) [(\mathbf{N} \times \mathbf{n}^{\beta}) \cdot (\mathbf{N} \times \mathbf{n}^{\alpha})] \quad (53)$$

In the same way, the following relation arises between the perturbations in stress and velocity gradient:

$$\delta \dot{\boldsymbol{\sigma}} = \mathbf{L}(\eta, \bar{k}, \mathbf{N}) : \delta \dot{\mathbf{U}},$$

with:

$$\mathbf{L}(\eta, \bar{k}, \mathbf{N}) = \mathbf{C} - \sum_{\alpha, \beta} \mathbb{S}_{\alpha\beta}^{-1}(\eta, \bar{k}, \mathbf{N}) (\mathbf{C} : \hat{\mathbf{S}}^{\alpha}) \otimes (\mathbf{C} : \hat{\mathbf{S}}^{\beta}). \quad (54)$$

For a given wave number \bar{k} , one can seek band type eigenmodes for all directions \mathbf{N} ; each of them is characterized by its growth rate η and displacement direction \mathbf{M} such that:

$$(\mathbf{N} \cdot \mathbf{L}(\eta, \bar{k}, \mathbf{N}) \cdot \mathbf{N}) \cdot \mathbf{M} = 0. \quad (55)$$

3. Active slip systems under uniform prescribed deformation and symmetry breaking.

This section focuses on the investigation of uniform deformation paths in equi-biaxial stretching for different crystal orientations and of the evolution of activated slip systems. To this aim, simulation is performed with an element free Galerkin numerical code using a finite deformation Lagrangian formalism (cf. Dequiedt et al., 2015) but which amounts to the constitutive relations

of Section 2.1 for small strains (same coefficients for the single crystal constitutive model). The evolution of slip system activation is displayed in Section 3.1 with emphasis on symmetric lattice orientations; the onset of symmetry breaking paths is analyzed in Section 3.2 in the light of the instability analysis of Section 2.2.

3.1. Slip system activation.

A copper single crystal is loaded in the two orthogonal directions x and y ($\varepsilon_{xx} = \varepsilon_{yy} = \varepsilon$) at a strain rate $\dot{\varepsilon} = 1 \text{ s}^{-1}$. The deformation is supposed to be isochoric ($\varepsilon_{zz} = -2\varepsilon$) and crystal orientations associated with different locations of direction z in the standard triangle of the crystal pole figure are considered.

Slip systems are denoted with the notations of Schmid and Boas (1935) for FCC crystals, in which capital letters are for slip plane normal and integers for slip directions (Table 4). In accordance with Section 2, they are oriented in such a way as to provide positive shearing rates for all cases considered in this work.

A crystal plasticity simulation of a cubic volume under imposed uniform deformation is performed. Direction z is tuned along one line crossing the standard triangle from the (001) / (011) axis to the (001) / ($\bar{1}11$) axis of the pole figure as depicted on Fig. 1: the related crystal orientations are numbered from 1 to 17.

First, both bounding points on the two axes, corresponding to z aligned with the (023) (orientation 1) and ($\bar{2}23$) (orientation 17) lattice axes, are investigated. The evolution of the shearing rates of active systems with ε for the two orientations is reported on Fig. 2. At the beginning of loading, the shearing rates are in accordance with the symmetry of the lattice with

respect to the loading axis, leading to the activation of more than the five necessary systems to accommodate any deformation and, of several collinear pairs. Namely, for orientation (023) , systems A3 and B4 are symmetric and display equal shearing rates just as systems A6 and B5, C3 and D4, C5 and D6 (these eight systems form the four collinear pairs A3/C3, B4/D4, B5/C5 and A6/D6). For orientation $(\bar{2}23)$, equal shearing rates are identified for symmetric systems B4 and C1, B5 and C5, D1 and D4 (these six systems form the three collinear pairs C1/D1, B4/D4 and B5/C5). Incidentally, for both cases, shearing rates are very close to the ones which would be obtained with a uniform interaction matrix (all the coefficients having the same value $a^{\alpha\beta} = 0.122$) as is illustrated on Fig. 2. However, for the DD driven matrix case contrary to the uniform matrix case, an evolution to a non-symmetric loading path occurs reducing by the same way the number of active systems and the co-activation of collinear systems with both high shearing rates. Namely, for orientation (023) , this departure increases the shearing rates of systems A6 and C5 and decreases the shearing rates of systems B5 and D6; it is followed by an evolution of the four other systems leading to a complete deactivation of systems B5, C3 and D4 and leaving very low shearing rate for system D6. For orientation $(\bar{2}23)$, the departure increases the shearing rates of systems B4, C5 and D1, decreases the shearing rate of systems B5 and C1 and leads to extinction of system D4.

Table 4

Slip plane normal \mathbf{n}^α and oriented slip direction $\hat{\mathbf{m}}^\alpha$ in the cubic lattice coordinate system with the notation of Schmid and Boas (1935) (in the \mathbf{n}^α and $\hat{\mathbf{m}}^\alpha$ columns, the sets of coordinate have to be divided by $\sqrt{3}$ and $\sqrt{2}$ respectively to preserve normality of vectors).

Slip System α	$\mathbf{n}^\alpha (\times \sqrt{3})$	$\hat{\mathbf{m}}^\alpha (\times \sqrt{2})$
A2	$(\bar{1}11)$	$(01\bar{1})$
A3		$(\bar{1}0\bar{1})$
A6		$(\bar{1}\bar{1}0)$
B2	(111)	$(01\bar{1})$
B4		$(10\bar{1})$
B5		$(1\bar{1}0)$
C1	$(11\bar{1})$	(011)
C3		$(\bar{1}0\bar{1})$
C5		$(\bar{1}10)$
D1	$(1\bar{1}1)$	(011)
D4		$(\bar{1}01)$
D6		$(\bar{1}\bar{1}0)$

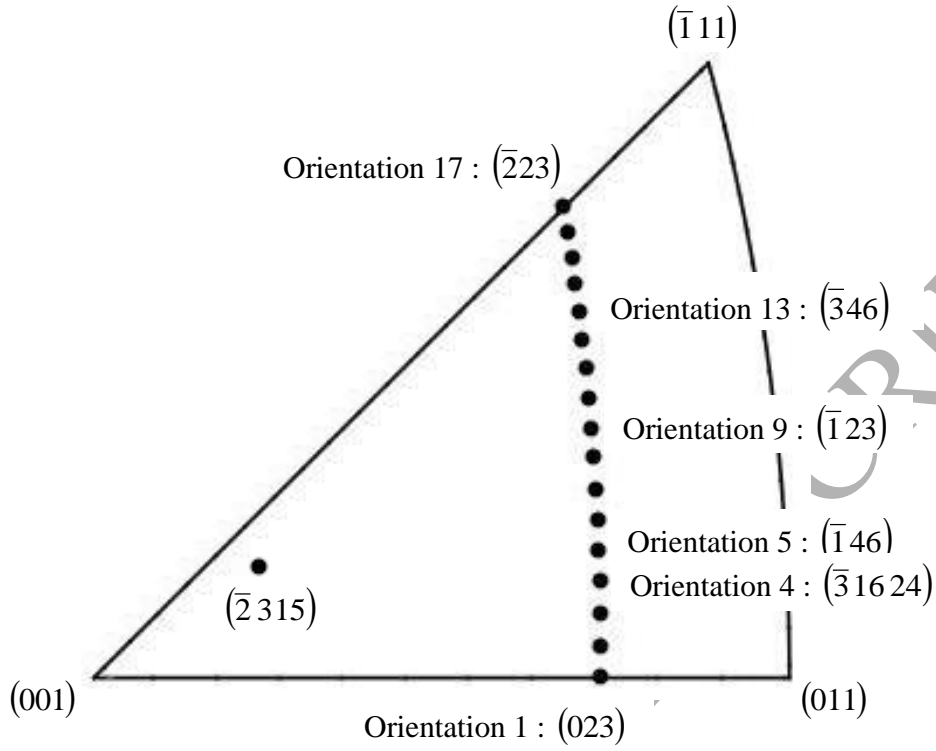


Fig. 1: Definition of crystal orientations: positions of the z-axis for 17 orientations on one line crossing the standard triangle and for orientation $(\bar{2} 315)$ considered in Section 4.

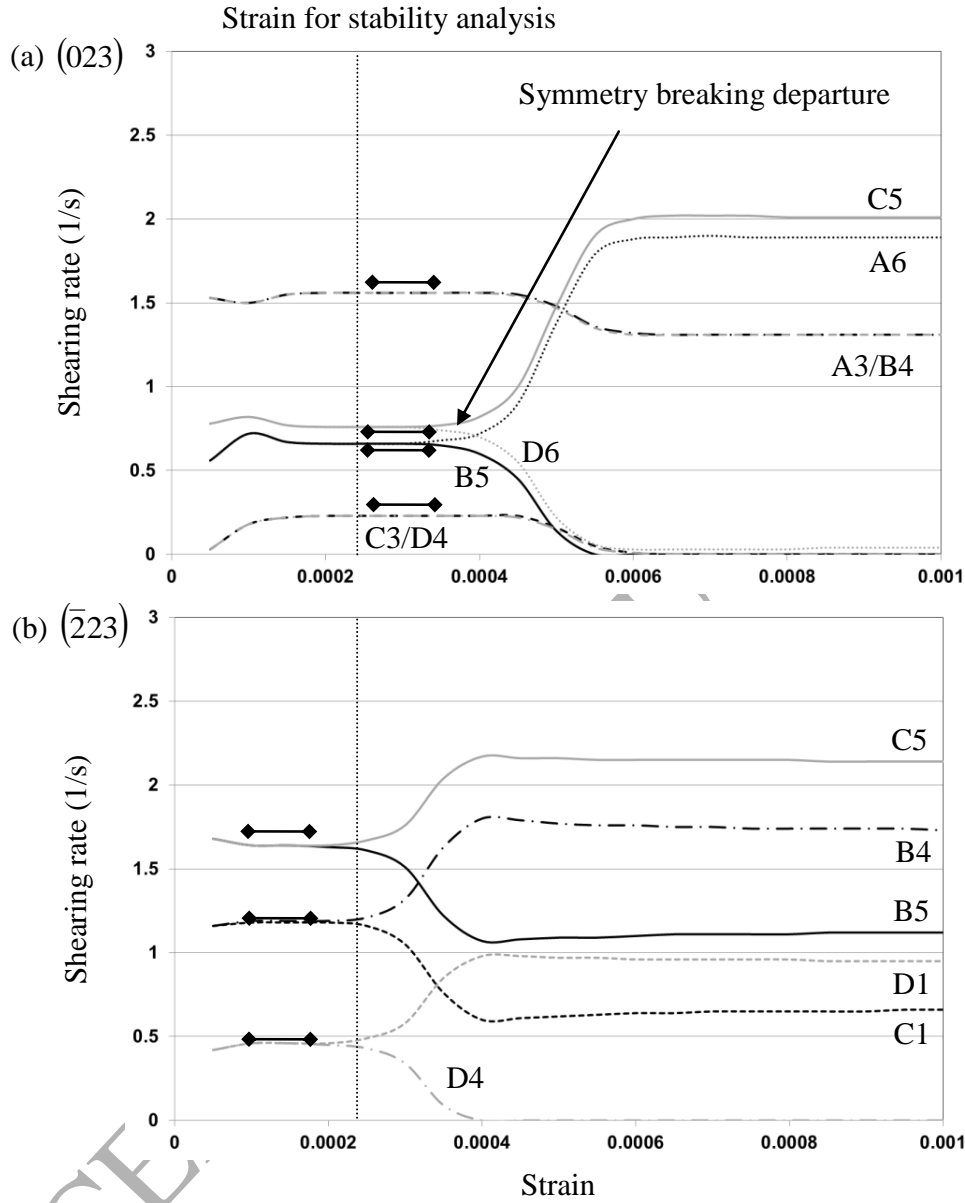


Fig. 2: Evolution of shearing rates with biaxial strain ε for the DD driven interaction matrix and for the two orientations (a) (023) and (b) ($\bar{2}23$). Symmetry breaking evolution is exhibited. Shearing rates for the uniform matrix case are settled with the horizontal diamond bounded bars; each bar relates to the closest pair of systems initially activated with the same shearing rate. The time for the instability analysis performed in Section 3.2 is also located on the graph.

Loading orientations inside the standard triangle are next considered. For small deformations, after a very short elastic-plastic transition, shearing rates slightly evolve before stabilizing. The uniform and DD driven interaction matrix cases exhibit substantially different system activation. The evolution of shearing rates with loading orientation for the two matrices are plotted on Fig. 3-a and 3-b respectively for a deformation $\varepsilon = 0.005$ for which these rates are almost time independent. The simulations using the DD driven interaction matrix exhibit a lower number of activated systems and at most two pairs of collinear systems for each orientation (versus three or four for the simulations using the uniform interaction matrix), confirming the propensity of the crystal to avoid the co-activation of a great number of systems and especially cross-slip pairs. Incidentally, although no departure arises on the loading path for each of these orientations, abrupt changes of the shearing rates are displayed between neighboring orientations (4 and 5 for instance).

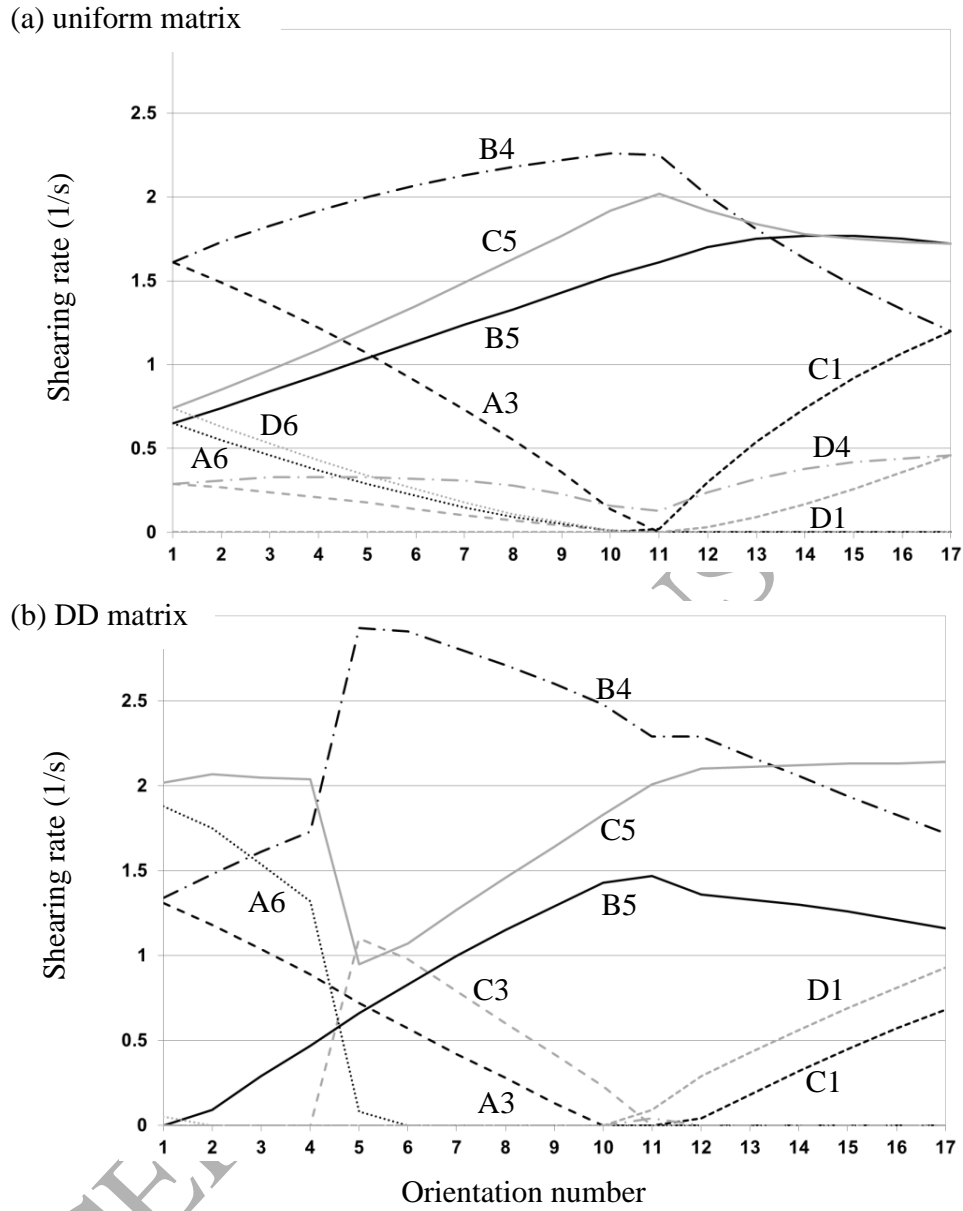


Fig. 3: Shearing rates for the different crystal orientations and after a biaxial deformation $\varepsilon = 0.005$: (a) uniform and (b) DD driven interaction matrix. The same line style is used for collinear systems.

3.2. Instability analysis.

The onset of symmetry breaking displayed for the two symmetric orientations is searched in the form of uniform instability modes (satisfying Eqs. (31) and (32)) of the symmetric evolution observed in the first part of the curves. Even though the departures do not arise exactly at the same time, the modes are evaluated for $\varepsilon = 0.00025$ for the two cases. Modes with positive growth rates η are found for both orientations (023) and ($\bar{2}23$). The growth rates and shearing rate perturbations are reported in Table 5.

Table 5

Instability modes and related shearing rate perturbations for orientations (023) and ($\bar{2}23$). Modes are reported in such a way that the vector of $\delta\hat{\gamma}^\alpha$ is normalized ($\sum_\alpha (\delta\hat{\gamma}^\alpha)^2 = 1$) and therefore only the ratio between shearing rates is significant.

Orientation of z-axis	(023)	($\bar{2}23$)	
	Mode I	Mode II	
Growth rate η (s ⁻¹)	27787	14985	36148
$\delta\hat{\gamma}^{B5}$	0.50	0.02	0.41
$\delta\hat{\gamma}^{B4}$	0	-0.53	-0.42
$\delta\hat{\gamma}^{C5}$	-0.50	0.02	-0.41
$\delta\hat{\gamma}^{C3}$	0	-0.51	-
$\delta\hat{\gamma}^{C1}$	-	-	0.42
$\delta\hat{\gamma}^{A6}$	-0.50	0.02	-
$\delta\hat{\gamma}^{A3}$	0	0.49	-
$\delta\hat{\gamma}^{D6}$	0.50	0.02	-
$\delta\hat{\gamma}^{D4}$	0	0.47	0.40
$\delta\hat{\gamma}^{D1}$	-	-	-0.40

For orientation (023), the first mode (mode I) displays perturbations of opposite sign for the slip rates A6/C5 on the one hand and B5/D6 on the other hand: this mode is the dominant one (higher growth rate) and controls the onset of the first symmetry breaking evolution observed on Fig. 2-a.

A second mode (mode II) with lower growth rate displays perturbations of opposite sign for the slip rates of systems A3/D4 on the one hand and B4/C3 on the other hand but does not seem to be triggered. For orientation $(\bar{2}23)$, the instability mode displays perturbations for systems B4, C5 and D1 in opposite sign with perturbations for systems B5, C1 and D4, and controls the symmetry breaking evolution observed on Fig. 2-b.

The influence of the interaction matrix on the selection of slip systems under prescribed uniform deformation has been demonstrated in this section (by comparison between a uniform and a DD driven matrix). The effect of slip system interactions is to limit the number of activated systems and, above all, the co-activation of cross slip pairs with the strongest interaction. Specifically, the evolution of symmetric configurations displays the onset of non-symmetric paths which can be analyzed as being driven by instability modes of the initial symmetric multi-slip loading paths.

4. Segregation modes for stable uniform deformation paths and non-local effects.

The aim of this section is to investigate the potential segregation of slip systems from the uniform deformation paths identified in Section 3 with the DD driven interaction matrix. Segregation is supposed to be triggered by plane wave instability modes of the uniform deformation as defined in Section 2.2. Special attention is paid to non-local effects which tend to penalize non-uniform system activation each time they induce plastic strain incompatibilities and therefore accumulation of GND densities. In this aim, we compare large wavelength modes, for which the non-local part of the constitutive law is inactive to finite wavelength modes for which gradient terms cannot be neglected.

Four orientations are considered and stability analysis is achieved at a deformation $\varepsilon = 0.005$ for which a stable uniform loading path is attained for all orientations (see Section 3). Section 4.1 is devoted to orientation $(\bar{3}1624)$ for which one pair of collinear systems is activated. Section 4.2 deals with orientation $(\bar{1}46)$ for which two collinear pairs co-exist. Section 4.3 addresses the case of orientation $(\bar{2}315)$, not considered in Section 3 but displayed in Dequiedt et al. (2015), for which no collinear pair is activated. For the symmetric loading orientation (023) , segregation modes still exist even after switching to the stable uniform path: this case is detailed in Appendix A.

4.1. Segregation modes for orientation $(\bar{3}1624)$.

For this loading orientation, systems A3, A6, B4, and collinear B5 and C5 are activated with respective shearing rates (evaluated for $\varepsilon = 0.005$): $\hat{\gamma}^{A3} = 0.89 \text{ s}^{-1}$, $\hat{\gamma}^{A6} = 1.32 \text{ s}^{-1}$, $\hat{\gamma}^{B4} = 1.73 \text{ s}^{-1}$, $\hat{\gamma}^{B5} = 0.47 \text{ s}^{-1}$, $\hat{\gamma}^{C5} = 2.04 \text{ s}^{-1}$. Plane wave modes with wavelength much larger than the length scale parameter L are first considered: in such a case, non-local effects can be disregarded ($\bar{k} = 0$) and the modes are given by Eq. (36). For many wave orientations \mathbf{N} , instability modes (such that $\text{Re}(\eta) > 0$) are identified. The maximum growth rate η (which is systematically real when positive) is mapped on Fig. 4 as a function of \mathbf{N} , set by angles θ and φ in the crystal axes⁶. Two peaks are identified on the map corresponding to two dominant band orientations I and Ib: the growth rate, band orientation \mathbf{N} , displacement direction \mathbf{M} and shearing rates $\delta\hat{\gamma}^\alpha$ of each of these two modes are summarized in Table 6.

⁶ In Dequiedt et al. (2015), the wave orientation was set in the loading axes for comparison with numerical simulation.

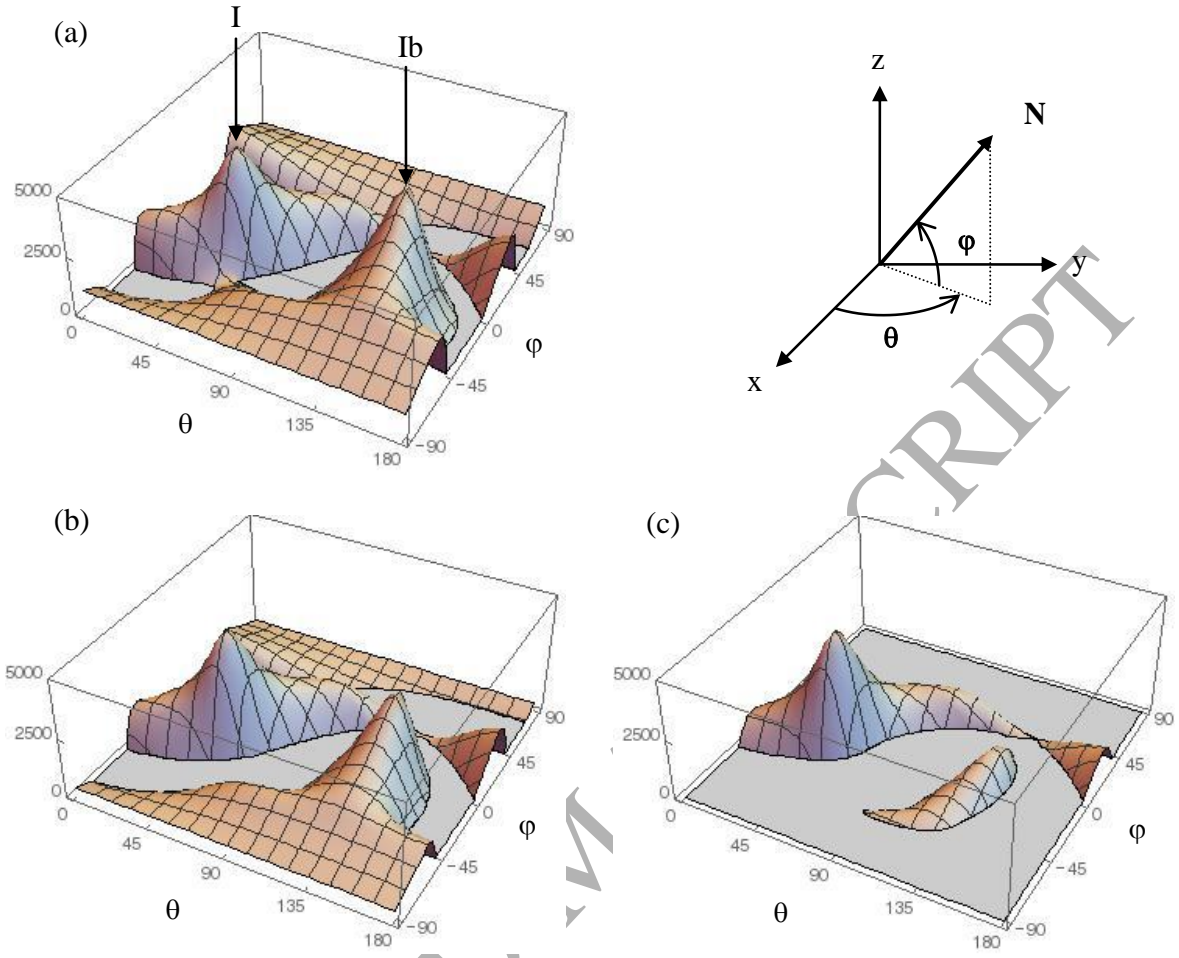


Fig. 4: Growing rate as a function of band orientation for crystal orientation $(\bar{3} 16 24)$ and wavenumbers (a) $\bar{k} = 0$ (dominant modes I and Ib are pointed) (b) $\bar{k} = 0.05$ and (c) $\bar{k} = 0.1$. Only positive growing rates are plotted.

Table 6

Characteristics of the dominant instability modes for crystal orientation $(\bar{3}1624)$ in the large wavelength limit ($\bar{k} = 0$). The shearing rates $\delta\tilde{\gamma}^\alpha$ defined in Eq. (34) are given with convention $\delta\tilde{\nu} = 1$ in Eq. (33).

Band orientation	η (s ⁻¹)	θ	φ	N	M
I	4744	45.1	-12.7	(0.69; 0.69; -0.22)	(0.70; -0.71; -0.03)
Ib	4472	134.9	1.2	(-0.71; 0.71; 0.01)	(-0.67; -0.68; 0.30)

Band orientation	$\delta\tilde{\gamma}^{A3}$	$\delta\tilde{\gamma}^{A6}$	$\delta\tilde{\gamma}^{B4}$	$\delta\tilde{\gamma}^{B5}$	$\delta\tilde{\gamma}^{C5}$
I	0	0.06	-0.01	0.37	-0.76
Ib	-0.01	0.04	0	0.31	-0.83

These two modes are dominated by perturbations of opposite sign for shearing rates $\hat{\gamma}^{B5}$ and $\hat{\gamma}^{C5}$ which initiate the segregation of the two collinear systems B5 and C5; the perturbations on the shearing rates of the other systems are much lower. As has already been noticed in Dequiedt et al. (2015), these two modes are nearly orthogonal in the sense that the band orientation of mode I is nearly orthogonal to its glide direction which is nearly collinear with the band orientation of mode Ib. This may be connected with the results of instability analysis for single slip crystal plasticity (Asaro and Rice, 1977 for instance): two band orientations are identified for the same yield condition, one with the normal to the band nearly collinear with the slip plane normal (usually called “slip band”) and the other with the slip direction (usually called “kink band”), the two localization modes differing by a pure lattice rotation.

When the wavelength is decreased and becomes of the same order as the length scale parameter L , non-local effects have to be introduced in the instability analysis. Plane wave instability modes are then given by Eq. (55). The maps of growth rates are displayed on Fig. 4 for the two non-dimensional wave numbers $\bar{k} = 0.05$ and 0.1. The domain of wave orientations for which

positive growth rates exist shrinks when \bar{k} increases. Two peaks are still displayed from the maps with orientations very close to mode I and Ib. The characteristics of these two modes are given in Table 7 for $\bar{k} = 0.1$. The shearing rate perturbations are almost the same as for $\bar{k} = 0$ even though for mode Ib, the perturbation involves non negligible shearing rates on systems A3 and B4 in addition to systems B5 and C5.

Whereas the growth rate of mode I is nearly unaffected by gradient effects, the growth rate of mode Ib strongly decreases when \bar{k} increases. If \bar{k} is increased up to 0.15, only mode I remains. A measure of the GND density linked with each of these modes (i.e., with the combination of shearing rate perturbations) is the norm of $\delta\tilde{\mathbf{G}}$ in which, owing Eq. (51):

$$\delta\dot{\mathbf{G}} = -k^2 \delta\tilde{\mathbf{G}} \exp(ik(\mathbf{x} \cdot \mathbf{N})) \exp(\eta t), \quad \text{and} \quad \delta\tilde{\mathbf{G}} = \sum_{\beta} \delta\tilde{\gamma}^{\beta} (\hat{\mathbf{m}}^{\beta} \otimes (\mathbf{N} \times \mathbf{n}^{\beta})) \quad (56)$$

$\|\delta\tilde{\mathbf{G}}\|$ is also reported in Table 7. For positive wavenumber \bar{k} , it is much higher for mode Ib than

for mode I for which it is negligible. This can be understood in the following way. The combination of perturbations on the two collinear systems (such that $\hat{\mathbf{m}}^{C5} = -\hat{\mathbf{m}}^{B5}$), which is the main component of the plastic transformation rate perturbation $\delta\dot{\mathbf{U}}^p$, expresses in the form of a single outer product which, for mode I, yields an almost curl free plastic transformation rate.

Namely:

$$\begin{aligned} \delta\dot{\mathbf{U}}^p &\approx \delta\hat{\gamma}^{B5} (\hat{\mathbf{m}}^{B5} \otimes \mathbf{n}^{B5}) + \delta\hat{\gamma}^{C5} (\hat{\mathbf{m}}^{C5} \otimes \mathbf{n}^{C5}) \\ &= ik [\hat{\mathbf{m}}^{B5} \otimes (\delta\tilde{\gamma}^{B5} \mathbf{n}^{B5} - \delta\tilde{\gamma}^{C5} \mathbf{n}^{C5})] \exp(ik(\mathbf{x} \cdot \mathbf{N})) \exp(\eta t) \end{aligned} \quad (57)$$

Since $\mathbf{M} \approx \mathbf{m}^{B5}$ and $\mathbf{N} \approx (\delta\tilde{\gamma}^{B5} \mathbf{n}^{B5} - \delta\tilde{\gamma}^{C5} \mathbf{n}^{C5})$:

$$\delta \dot{\mathbf{G}} = \mathbf{curl}(\delta \dot{\mathbf{U}}^p) \quad \text{gives} \quad \delta \tilde{\mathbf{G}} \approx \mathbf{M} \otimes (\mathbf{N} \times \mathbf{N}) = 0 \quad (58)$$

On the contrary, for mode Ib: $\mathbf{N} \approx \mathbf{m}^{B5}$ and $\mathbf{M} \approx (\delta \tilde{\gamma}^{B5} \mathbf{n}^{B5} - \delta \tilde{\gamma}^{C5} \mathbf{n}^{C5})$ and, subsequently:

$$\delta \tilde{\mathbf{G}} \approx \mathbf{N} \otimes (\mathbf{M} \times \mathbf{N}) \neq 0. \quad (59)$$

The same property has been displayed for single slip localization: the non-local effects have no incidence on the onset of slip bands whereas they penalize the formation of kink bands. This has been developed by Forest (1998) using the Cosserat theory of plasticity for non-local effects.

Table 7

Characteristics of the dominant instability modes for crystal orientation $(\bar{3}1624)$ and wavenumber $\bar{k} = 0.1$.

Band orientation	$\eta \text{ (s}^{-1}\text{)}$	θ	φ
I	4748	45.1	-12.7
Ib	1258	131.5	-0.1

Band orientation	$\delta \tilde{\gamma}^{A3}$	$\delta \tilde{\gamma}^{A6}$	$\delta \tilde{\gamma}^{B4}$	$\delta \tilde{\gamma}^{B5}$	$\delta \tilde{\gamma}^{C5}$	$\ \delta \tilde{\mathbf{G}}\ $
I	0	0.03	0	0.38	-0.77	0.03
Ib	0.14	-0.02	-0.15	0.44	-0.77	0.98

4.2. Segregation modes for orientation $(\bar{1}46)$.

For this loading orientation, systems A3, A6, B4, B5, C3, C5 are activated (hence including the collinear pairs A3/C3 and B5/C5) with respective shearing rates (evaluated for $\varepsilon = 0.005$):

$$\hat{\gamma}^{A3} = 0.72 \text{ s}^{-1}, \hat{\gamma}^{A6} = 0.08 \text{ s}^{-1}, \hat{\gamma}^{B4} = 2.93 \text{ s}^{-1}, \hat{\gamma}^{B5} = 0.66 \text{ s}^{-1}, \hat{\gamma}^{C3} = 1.10 \text{ s}^{-1}, \hat{\gamma}^{C5} = 0.95 \text{ s}^{-1}. \text{ In the}$$

large wavelength limit ($\bar{k} = 0$), instability modes emerge for any orientation as can be seen on

Fig. 5. Although the growing rate map is rather smooth, three pairs of nearly orthogonal local

maxima can be identified, one of them associated with the segregation of systems B5 and C5

(modes I and Ib), one with the segregation of systems A3 and C3 (modes III and IIIb) and the last

one (modes II and IIb) implying a combination of perturbations on all the systems, shearing rate perturbations on collinear systems still being of opposite sign. The characteristics of these six modes are reported in Table 8.

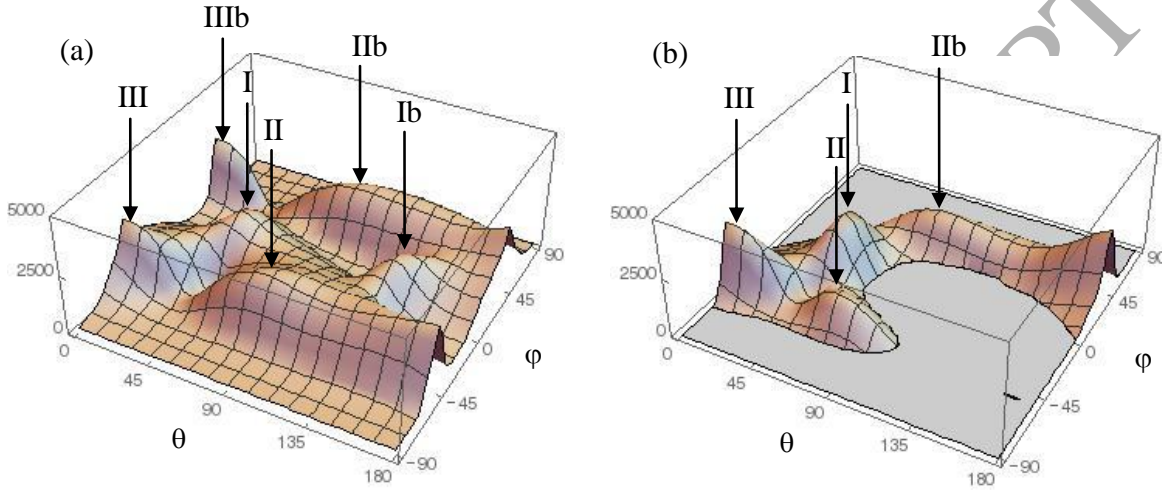


Fig. 5: Growing rate as a function of band orientation for crystal orientation $(\bar{1}46)$ and wavenumbers (a) $\bar{k} = 0$ and (b) $\bar{k} = 0.1$. The dominant modes are still pointed.

Table 8

Characteristics of the dominant instability modes for crystal orientation $(\bar{1}46)$ in the large wavelength limit ($\bar{k} = 0$).

Band orientation	η (s ⁻¹)	θ	φ	N	M
I	2421	45.7	-2.2	(0.70; 0.71; -0.04)	(0.71; -0.70; -0.05)
Ib	2422	135.8	2.0	(-0.72; 0.70; 0.03)	(-0.69; -0.72; 0.05)
II	2623	89.0	-42.0	(0.01; 0.74; -0.67)	(-0.09; 0.67; 0.74)
IIb	2616	98.0	47.8	(-0.09; 0.67; 0.74)	(0.04; 0.75; -0.66)
III	2928	5.3	-44.7	(0.71; 0.07; -0.70)	(0.70; 0.01; 0.71)
IIIb	2903	1.2	45.7	(0.70; 0.01; 0.71)	(0.70; 0.11; -0.70)

Band orientation	$\delta\tilde{\gamma}^{A3}$	$\delta\tilde{\gamma}^{A6}$	$\delta\tilde{\gamma}^{B4}$	$\delta\tilde{\gamma}^{B5}$	$\delta\tilde{\gamma}^{C3}$	$\delta\tilde{\gamma}^{C5}$
I	-0.03	0	0.11	0.54	0.08	-0.69
Ib	-0.04	0	0.10	0.54	0.07	-0.69
II	0.67	0.01	-0.29	-0.52	-0.83	0.70
IIb	0.65	0.01	-0.31	-0.49	-0.86	0.73
III	0.54	0.01	0	0.01	-0.68	0.02
IIIb	0.50	0	0.02	0	-0.70	0.01

When the wavenumber is increased, the extent of the instability domain in band orientation is drastically reduced. For $\bar{k} = 0.1$, among the six dominant modes only four remain (Table 9). As for orientation $(\bar{3}1624)$, for mode pairs concerning the segregation of one pair of collinear systems (I / Ib and III / IIIb), one of the two is nearly unaffected by non-local effects whereas the second is eliminated; modes implying combination of perturbations on all systems (II and IIb) are both stabilized by non-local effects; their orientation and the amplitude of the different shearing rate perturbations is slightly modified. These results are in agreement with the norm of the dislocation density tensor $\delta\tilde{\mathbf{G}}$.

Table 9

Characteristics of the dominant instability modes for crystal orientation $(\bar{1}46)$ and wavenumber $\bar{k} = 0.1$.

Band orientation	η (s ⁻¹)	θ	φ
I	2418	45.1	-2.6
-	-	-	-
II	1465	67.9	-44.1
IIb	1488	82.3	43.4
III	2928	5.4	-44.7
-	-	-	-

Band orientation	$\delta\tilde{\gamma}^{A3}$	$\delta\tilde{\gamma}^{A6}$	$\delta\tilde{\gamma}^{B4}$	$\delta\tilde{\gamma}^{B5}$	$\delta\tilde{\gamma}^{C3}$	$\delta\tilde{\gamma}^{C5}$	$\ \delta\tilde{\mathbf{G}}\ $
I	0	0	0.05	0.55	0.05	-0.68	0.03
-	-	-	-	-	-	-	-
II	0.32	-0.02	0.15	-0.39	-0.73	0.74	0.48
IIb	0.43	-0.04	0.29	-0.59	-0.51	0.57	0.68
III	0.54	0.01	0	0.01	-0.68	0.02	0.01
-	-	-	-	-	-	-	-

As a conclusion, when several collinear pairs are involved, many segregation modes can be activated implying different combinations of these systems; in this case, the non-local effects operate a strong selection among these modes in a way that minimizes the accumulation of GND induced by the heterogeneous deformation. Modes implying the dissociation of a single collinear pair for which the plastic strain rate is almost curl free (cf. Eq. (57)) and does not need to be accommodated by GND densities, are thus favored.

4.3. Segregation modes for orientation $(\bar{2}315)$.

For this loading orientation, systems A2, A3, B4, C1, C5 and D6 are activated with respective

shearing rates (evaluated for $\varepsilon = 0.005$): $\hat{\gamma}^{A2} = 0.87 \text{ s}^{-1}$, $\hat{\gamma}^{A3} = 1.17 \text{ s}^{-1}$, $\hat{\gamma}^{B4} = 1.37 \text{ s}^{-1}$,

$\hat{\gamma}^{C1} = 1.06 \text{ s}^{-1}$, $\hat{\gamma}^{C5} = 0.08 \text{ s}^{-1}$, $\hat{\gamma}^{D6} = 0.13 \text{ s}^{-1}$. Collinear interaction is not involved and the

dislocations of non-coplanar systems form Hirth locks, Lomer locks and glissile junctions. In the large wavelength limit ($\bar{k} = 0$), instability modes do exist but for a limited domain of band orientations as can be seen on Fig. 6 and the growth rates are lower than for the two former cases involving collinear systems: the two dominant modes I and Ib (cf. Table 10) tend to activate in phase systems forming Hirth locks (A3/B4 and A2/C1) and dissociate coplanar systems (A2/A3) and systems forming glissile junctions (A2/B4 and A3/C1) and Lomer locks (B4/C1). This is in accordance with the respective strength of these interactions (cf. Table 2)⁷.

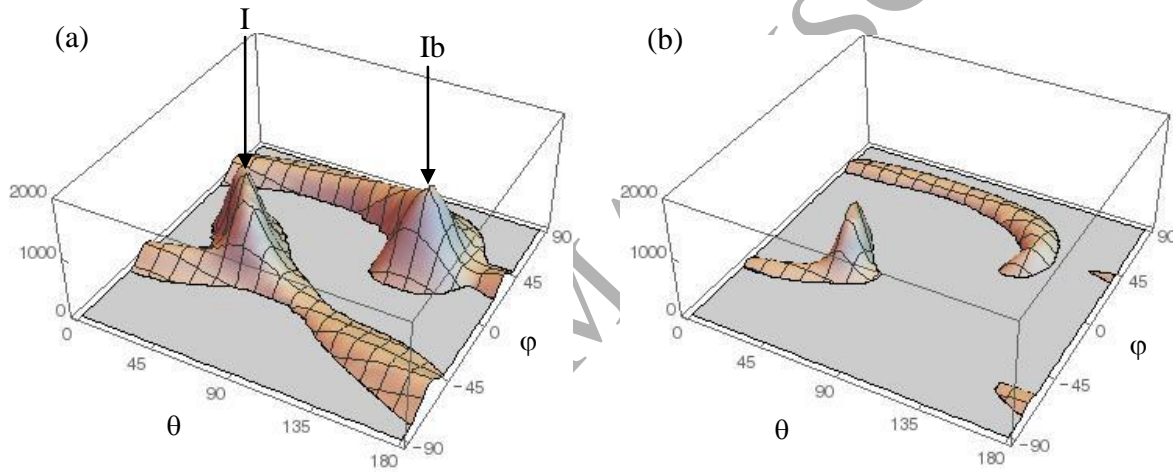


Fig. 6: Growing rate as a function of band orientation for crystal orientation $(\bar{2}315)$ and wavenumbers (a) $\bar{k} = 0$ (modes I and Ib are pointed) and (b) $\bar{k} = 0.1$.

⁷ As has been mentioned in Dequiedt et al. (2015), the intensity of the dipolar interaction is estimated with less accuracy than the other ones. A dipolar interaction weaker than the Hirth lock ($a_1^{copla} < a_1^{ortho}$), which was found to be consistent with the experimental results of Dmitrieva et al. (2009), would probably modify the segregation of systems.

Table 10

Characteristics of the dominant instability modes for crystal orientation $(\bar{2}315)$ in the large wavelength limit ($\bar{k} = 0$).

Band orientation	η (s ⁻¹)	θ	φ	N	M	
I	1316	42.9	2.0	(0.73; 0.68; 0.03)	(-0.57; 0.59; 0.57)	
Ib	1313	134.4	34.8	(-0.57; 0.59; 0.57)	(0.74; 0.67; 0.06)	

Band orientation	$\delta\tilde{\gamma}^{A2}$	$\delta\tilde{\gamma}^{A3}$	$\delta\tilde{\gamma}^{B4}$	$\delta\tilde{\gamma}^{C1}$	$\delta\tilde{\gamma}^{C5}$	$\delta\tilde{\gamma}^{D6}$
I	0.46	-0.53	-0.49	0.51	0.01	0
Ib	0.44	-0.54	-0.49	0.51	0.01	0

For $\bar{k} = 0.1$, the domain of positive growth rates is extremely limited and the growth rate of both modes I and Ib is reduced (Table 11). Mode I is the less affected of the two and implies the same systems as in the long wavelength case ($\bar{k} = 0$) with slightly different amplitudes for the shearing rate perturbations. Mode Ib is much more “stabilized” and has evolved towards a mode dominated by the dissociation of the coplanar pair A2/A3, the other systems playing a secondary role. The norms of the dislocation density tensors $\|\delta\tilde{\mathbf{G}}\|$ associated with the two modes are comparable. If \bar{k} is increased up to 0.2, mode Ib is even more stabilized and prominence of systems A2 and A3 has been reinforced (see Table 11); this evolution is accompanied by a decrease of $\|\delta\tilde{\mathbf{G}}\|$ which means that this combination of systems limits plastic strain field incompatibility. One can observe that, as for collinear systems, a pure combination of two coplanar systems also yields a curl free plastic strain rate perturbation, provided that the normal to the bands is aligned with the normal to their common slip plane ($\mathbf{n}^{A2} = \mathbf{n}^{A3}$ in the present case), which is not far from being the case for mode Ib. Namely, if:

$$\begin{aligned}\delta\dot{\mathbf{U}}^p &\approx \delta\hat{\gamma}^{A2}(\hat{\mathbf{m}}^{A2} \otimes \mathbf{n}^{A2}) + \delta\hat{\gamma}^{A3}(\hat{\mathbf{m}}^{A3} \otimes \mathbf{n}^{A3}) \\ &= ik \left[(\delta\tilde{\gamma}^{A2} \hat{\mathbf{m}}^{A2} + \delta\tilde{\gamma}^{A3} \hat{\mathbf{m}}^{A3}) \otimes \mathbf{n}^{A2} \right] \exp(ik(\mathbf{x} \cdot \mathbf{N})) \exp(i\eta t)\end{aligned}\quad (60)$$

and:

$$\mathbf{N} \approx \mathbf{n}^{A2}, \quad (61)$$

then:

$$\delta\tilde{\mathbf{G}} \approx (\delta\tilde{\gamma}^{A2} \hat{\mathbf{m}}^{A2} + \delta\tilde{\gamma}^{A3} \hat{\mathbf{m}}^{A3}) \otimes (\mathbf{N} \times \mathbf{N}) = 0, \quad (62)$$

which explains the decrease of $\|\delta\tilde{\mathbf{G}}\|$ with \bar{k} .

Table 11

Characteristics of the dominant instability modes for crystal orientation $(\bar{2}315)$ and wavenumber $\bar{k} = 0.1$ and of mode Ib for wavenumber $\bar{k} = 0.2$.

Band orientation	η (s ⁻¹)	θ	φ				
I	839	45.6	-3.9				
Ib	251	133.1	44.0				
Ib ($\bar{k} = 0.2$)	71	133.5	42.8				

Band orientation	$\delta\tilde{\gamma}^{A2}$	$\delta\tilde{\gamma}^{A3}$	$\delta\tilde{\gamma}^{B4}$	$\delta\tilde{\gamma}^{C1}$	$\delta\tilde{\gamma}^{C5}$	$\delta\tilde{\gamma}^{D6}$	$\ \delta\tilde{\mathbf{G}}\ $
I	0.43	-0.41	-0.56	0.66	0.02	-0.15	0.22
Ib	0.95	-0.79	-0.16	0.22	-0.06	-0.13	0.24
Ib ($\bar{k} = 0.2$)	1.04	-0.93	-0.03	0.08	-0.03	-0.12	0.075

5. Conclusion.

The influence of slip system interactions on the deformation of single crystals is investigated in this work at the scale of continuum including both local and non-local approaches. The propensity to accommodate the deformation by a mean that minimizes strain hardening was found to bring instability of loading paths involving combinations of strongly interacting slip systems and to trigger their evolution towards more favorable configurations. The need for an accurate evaluation of the intensity of the different interactions, as can be done by DD simulations, is emphasized. On the one hand, the hierarchy of interactions influences slip system selection under prescribed uniform deformation and, in some cases, yields instability of symmetric multi-slip configurations which shift into non-symmetric activation paths.

On the other hand, strong interactions favor the development of heterogeneous deformation of the single crystal linked to the segregation of systems in separated zones. Laminar segregation patterns are justified as being triggered by plane wave eigenmodes of the homogeneous deformation path. Instability modes of various orientations could be found, the dominant ones involving once again the strongest interacting systems. In the case of FCC crystals, crucial role is played by the collinear interaction between cross slip pairs, segregation being ruled by the order of the other interactions when no such pair is activated. Incidentally, the perturbed solutions predicted by the dominant eigenmodes have strong connections with the bifurcations identified in the rate-independent case by different authors (Petryk and Kurska, 2013, Kratochvil and Kruzik, 2015), even though the complete interaction matrix provides further information; still, the two approaches are not totally equivalent due to viscoplastic regularization adopted here.

Gradient plasticity effects, coming from the accommodation of plastic strain field incompatibilities by geometrically necessary dislocations (GND), yield an additional selection among segregation modes. When the wavelength is decreased and becomes of the same order of the internal length scale of the gradient terms, the set of potential orientations for segregation modes is strongly reduced. Moreover, the dominant modes are stabilized differently depending on the induced plastic incompatibility. Each time the resulting plastic strain is nearly compatible (curl free), the mode is almost unaffected by gradient effects: this concerns for instance the single dissociation of either collinear or coplanar pairs. On the contrary, modes generating strong plastic strain field incompatibility are progressively extinguished. For stabilized modes, an evolution of the orientation and of the shearing rates of the different systems involved is also observed in a way that limits once again GND accumulation.

Yet, the former results lay on the assumption that non-local effects are properly modelled by the sole dislocation density tensor. More sophisticated models, for which back stresses are functions of a combination of the Burgers vectors and line directions of GND belonging to all systems (see for instance Bayley et al. (2006)), would probably slightly modify the conclusions concerning the evolution of segregation modes with gradient effects.

Acknowledgements:

The author is grateful to his colleagues C. Denoual, R. Madec for fruitful discussions and careful examination of the manuscript.

Appendix A. Segregation modes for orientation (023) on the non-symmetric loading path.

For this loading orientation, systems A3, A6, B4, C5 and D6 remain after symmetry breaking departure, the latter with a low intensity. Their respective shearing rates are for $\varepsilon = 0.005$:

$\dot{\gamma}^{A3} = 1.31 \text{ s}^{-1}$, $\dot{\gamma}^{A6} = 1.88 \text{ s}^{-1}$, $\dot{\gamma}^{B4} = 1.34 \text{ s}^{-1}$, $\dot{\gamma}^{C5} = 2.02 \text{ s}^{-1}$, $\dot{\gamma}^{D6} = 0.05 \text{ s}^{-1}$. In the large wavelength limit ($\bar{k} = 0$), instability modes do exist for most of the orientations as can be seen on Fig. A.1. Three pairs of local maxima are still identified (Table A.1). The two first modes (I and Ib) are dominated by shearing rate perturbations for system A6, the shearing rate perturbations for collinear system D6 being of opposite sign but of much lower amplitude. The two last ones (III and IIIb), exhibit shearing rate perturbations of the same order for systems A3, A6, B4 and C5; as has already been noticed for orientation $(\bar{2} \ 3 \ 15)$, perturbations have the same sign for systems forming Hirth lock and opposite sign for systems forming glissile junctions or Lomer locks. Modes II and IIb seem to be a combination of the two other pairs.

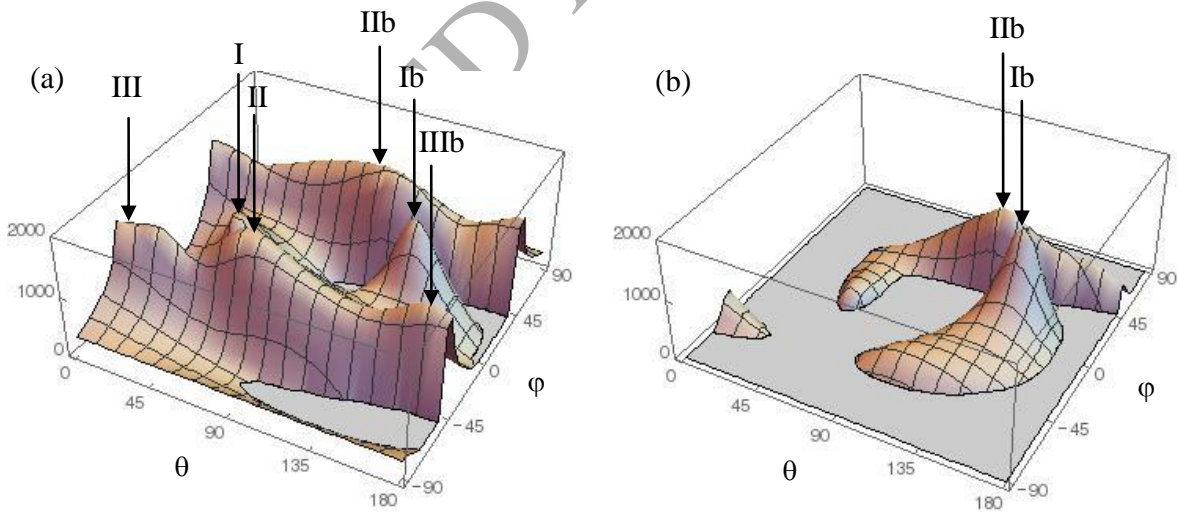


Fig. A.1: Growing rate as a function of band orientation for crystal orientation (023) and wavenumbers (a) $\bar{k} = 0$ and (b) $\bar{k} = 0.1$.

Table A.1

Characteristics of the dominant instability modes for crystal orientation (023) in the large wavelength limit ($\bar{k} = 0$).

Band orientation	η (s ⁻¹)	θ	φ	N	M
I	1441	47.4	-11.0	(0.66; 0.72; -0.19)	(-0.61; 0.67; 0.42)
Ib	1629	132.8	20.6	(-0.64; 0.69; 0.35)	(0.64; 0.72; -0.25)
II	1848	70.6	-37.2	(0.27; 0.75; -0.60)	(-0.32; 0.66; 0.68)
IIb	1792	107.6	46.3	(-0.21; 0.66; 0.72)	(-0.36; -0.74; 0.57)
III	1807	3.5	-47.2	(0.68; 0.04; -0.73)	(0.73; -0.05; 0.68)
IIIb	1799	-2.6	42.7	(0.73; -0.03; 0.68)	(-0.68; -0.07; 0.73)

Band orientation	$\delta\tilde{\gamma}^{A3}$	$\delta\tilde{\gamma}^{A6}$	$\delta\tilde{\gamma}^{B4}$	$\delta\tilde{\gamma}^{C5}$	$\delta\tilde{\gamma}^{D6}$
I	0.09	-0.91	0.11	0.17	0.11
Ib	0.13	-0.82	0.09	0.27	0.13
II	0.58	-1.25	0.42	-0.18	0.14
IIb	-0.41	1.30	-0.60	0.24	-0.13
III	0.61	-0.68	0.61	-0.78	0.09
IIIb	-0.58	0.69	-0.64	0.78	-0.08

The extent of the instability domain is still reduced when the wavenumber increases. For

$\bar{k} = 0.1$, only two of the dominant modes remain (modes Ib and IIb, cf. Table A.2). Their growth rates are reduced in accordance with the intensity of the dislocation density tensor.

Table A.2

Characteristics of the dominant instability modes for crystal orientation (023) and wavenumber $\bar{k} = 0.1$.

Band orientation	η (s ⁻¹)	θ	φ
Ib	1563	134.3	21.6
IIb	1376	116.6	40.1

Band orientation	$\delta\tilde{\gamma}^{A3}$	$\delta\tilde{\gamma}^{A6}$	$\delta\tilde{\gamma}^{B4}$	$\delta\tilde{\gamma}^{C5}$	$\delta\tilde{\gamma}^{D6}$	$\ \delta\tilde{\mathbf{G}}\ $
Ib	0.15	-0.87	0.03	0.18	0.15	0.17
IIb	-0.53	1.16	-0.43	0.05	-0.11	0.34

In this case of loading, the symmetry breaking departure should be followed by a segregation process; in other words, the crystal would first de-activate redundant systems and, in a second time, partially segregate the remaining ones in disconnected bands.

Notations:

Vectors and tensors are written in bold characters.

$\{\mathbf{A}\}_S$ is the symmetric part of tensor \mathbf{A} .

Second and fourth order tensor products and inner products are defined by:

$$(\mathbf{A} \cdot \mathbf{B})_{ij} = A_{ik} B_{kj}, \quad \mathbf{A} : \mathbf{B} = A_{ik} B_{ik}, \quad (\mathbf{C} : \mathbf{B})_{ij} = C_{ijkl} B_{kl}, \dots$$

The cross product of vectors is defined by (e_{ikl} is a component of the third order alternating Levi-Civita tensor):

$$(\mathbf{a} \times \mathbf{b})_i = e_{ikl} a_k b_l.$$

The **curl** operation on tensors is defined with the following convention:

$$(\mathbf{curl}(\mathbf{A}))_{ij} = e_{jkl} A_{il,k}.$$

References:

- Asaro, R.J., 1979. Geometrical effects in the inhomogeneous deformation of ductile single crystals. *Acta Metall.*, 27, 445-453.
- Asaro, R.J., Rice, J.R., 1977. Strain localization in ductile single crystals. *J. Mech. Phys. Solids*, 25, 309-338.

- Bayley, C.J., Brekelmans, W.A.M., Geers, M.G.D., 2006. A comparison of dislocation induced back stress formulations in strain gradient crystal plasticity, *Int. J. Solids Struct.*, 43, 7268-7286.
- Bigoni, D., Hueckel, T., 1991. Uniqueness and localization – I. Associative and non-associative elastoplasticity. *Int. J. Solids Struct.*, 28 (2), 197-213.
- Bigoni, D., Petryk, H., 2002. A note on divergence and flutter instabilities in elastic-plastic materials. *Int. J. Solids Struct.*, 39, 911-926.
- Busso, E.P., Cailletaud, G., 2005. On the selection of active slip systems in crystal plasticity. *Int. J. Plast.*, 21, 2212-2231.
- Cermelli, P., Gurtin, M.E., 2001. On the characterization of geometrically necessary dislocations in finite plasticity, *J. Mech. Phys. Solids*, 49, 1539-1568.
- Dequiedt, J.L., Denoual, C., Madec, R., 2015. Heterogeneous deformation in ductile FCC single crystals in biaxial stretching: the influence of slip system interactions. *J. Mech. Phys. Solids*, 83, 301-318.
- Dmitrieva, O., Dondl, P.W., Müller, S., Raabe, D., 2009. Lamination microstructure in shear deformed copper single crystals. *Acta Mater.*, 57, 3439-3449.
- Evers, L.P., Brekelmans, W.A.M., Geers, M.G.D., 2004. Non-local crystal plasticity model with intrinsic SSD and GND effects. *J. Mech. Phys. Solids*, 52, 2379-2401.
- Forest, S., 1998. Modeling slip, kink and shear banding in classical and generalized single crystal plasticity. *Acta Mater.*, 46 (9), 3265-3281.
- Franciosi, P., Berveiller, M., Zaoui, A., 1980. Latent hardening in copper and aluminium single crystals. *Acta Metall.*, 28, 273-283.

- Franciosi, P., Zaoui, A., 1982. Multislip tests on copper crystals: a junctions hardening effect. *Acta Metall.*, 30, 2141-2151.
- Groma, I., Csikor, F.F., Zaiser, M., 2003. Spatial correlations and higher-order gradient terms in a continuum description of dislocation dynamics. *Acta Mater.*, 51, 1271-1281.
- Gurtin, M.E., 2002. A gradient theory of single-crystal viscoplasticity that accounts for geometrically necessary dislocations. *J. Mech. Phys. Solids*, 50, 5-32.
- Gurtin, M.E., Needleman, A., 2005. Boundary conditions in small deformation, single crystal plasticity that account for the Burgers vector. *J. Mech. Phys. Solids*, 53, 1-31.
- Havner, K.S., Shalaby, A.H., 1977. A simple mathematical theory of finite distortional latent hardening in single crystals. *Proc. R. Soc. Lond.*, A358, 47-70.
- Hill, R., 1959. Some basic principles in the mechanics of solids without a natural time. *J. Mech. Phys. Solids*, 7, 209-225.
- Jin, N.Y., Winter, A.T., 1984. Cyclic deformation of copper single crystals oriented for double slip. *Acta Metall.*, 32 (7), 989-995.
- Kalidindi, S.R., Anand, L., 1993. Large deformation simple compression of a copper single crystal. *Metall. Trans. A* 24A, 989-992.
- Kratochvil, J., Kruzik, M., 2015. A crystal plasticity model of a formation of a deformation band structure. *Phil. Mag.*, 95 (32), 3621-3639.
- Kubin, L.P., 2013. Dislocations, mesoscale simulations and plastic flow. Oxford Series on Material Modelling, Oxford.
- Kubin, L., Devincere, B., Hoc, T., 2008. Modelling dislocation storage rates and mean free paths in face-centered cubic crystals. *Acta Mater.*, 56, 6040-6049.

- Kubin, L., Hoc, T., Devincere, B., 2009. Dynamic recovery and its orientation dependence in face-centered cubic crystals. *Acta Mater.*, 57, 2567-2575.
- Kuroda, M., Tvergaard, V., 2008. On the formulations of higher-order strain gradient crystal plasticity models. *J. Mech. Phys. Solids*, 56, 1591-1608.
- Madec, R., Devincere, B., Kubin, L., Hoc, T., Rodney, D., 2003. The role of collinear interaction in dislocation-induced hardening. *Science*, 301, 1879-1882.
- Madec, R., Kubin, L., 2017. Dislocation strengthening in FCC metals and in BCC metals at high temperatures. *Acta Mater.*, 126, 166-173.
- Molinari, A., 1988. Bandes de cisaillement dans un monocristal viscoplastique en traction simple. *C. R. Acad. Sci. Paris*, 306 (II), 841-846.
- Neilsen, M.K., Schreyer, H.L., 1993. Bifurcations in elastic-plastic materials. *Int. J. Solids Struct.*, 30 (4), 521-544.
- Nye, J.F., 1953. Some geometrical relations in dislocated solids. *Acta Metall.*, 1, 153-162.
- Ortiz, M., Repetto, E.A., 1999. Nonconvex energy minimization and dislocation structures in ductile single crystals. *J. Mech. Phys. Solids*, 47, 397-462.
- Petryk, H., Kurska, M., 2011. Selective symmetrization of the slip system interaction matrix in crystal plasticity. *Arch. Mech.*, 63 (3), 287-310.
- Petryk, H., Kurska, M., 2013. The energy criterion for deformation banding in ductile single crystals. *J. Mech. Phys. Solids*, 61, 1854-1875.
- Pierce, D., Asaro, R.J., Needleman, A., 1982. An analysis of nonuniform and localized deformation in ductile single crystals. *Acta Metall.*, 30, 1087-1119.
- Piercy, G.R., Cahn, R.W., Cottrell, A.H., 1955. A study of primary and conjugate slip in crystals of alpha-brass. *Acta Metall.*, 3, 331-338.

- Rice, J.R., 1976. The localization of plastic deformation. In: Koiter, W.T. (Ed.) Proceedings of the 14th International Congress on Theoretical and Applied Mechanics, North Holland Publishing Company, Amsterdam, pp. 207-220.
- Saimoto, S., 1963. Low temperature tensile deformation of copper single crystals oriented for multislip. Ph. D. thesis, M.I.T., Cambridge, MA.
- Schmid, E., Boas, W., 1935. Kristallplastizität, Berlin, Springer Verlag.
- Simmons, G., Wang, H., 1971. Single crystal elastic constants and calculated aggregate properties. The M.I.T. Press, Cambridge, Massachussets.
- Teodosiu, C., Raphanel, J.L., Tabourot, L., 1991. Finite element simulation of the large elastoplastic deformation. In: *Large Plastic Deformations* edited by Teodosiu C., Raphanel J.L. and Sidoroff F., Rotterdam, A.A. Balkema, pp. 153-168.
- Yalcinkaya, T., Brekelmans, W.A.M., Geers, M.G.D., 2012. Non-convex rate dependent strain gradient crystal plasticity and deformation patterning. *Int. J. Solids Struct.*, 49, 2625-2636.